



# Pauli resonance states in light nuclei: How they appear and how they can be eliminated

N. Kalzhigitov <sup>\*</sup>

*Department of Theoretical and Nuclear Physics, al-Farabi Kazakh National University, Almaty 050040, Kazakhstan*

V. S. Vasilevsky <sup>†</sup>

*Bogolyubov Institute for Theoretical Physics 14-b Metrolohichna str. Kyiv 03143, Ukraine*



(Received 10 November 2023; revised 29 February 2024; accepted 26 April 2024; published 14 May 2024)

A systematic analysis of parameters and properties of the Pauli resonance states is performed for light nuclei  ${}^6\text{Li}$ ,  ${}^7\text{Li}$ ,  ${}^8\text{Be}$ ,  ${}^9\text{Be}$ , and  ${}^{10}\text{B}$ , which are treated as two-cluster systems. The Pauli resonance states are redundant solutions of the resonating group method. They appear when one tries to use a more advanced description of the internal structure of interacting clusters. Our calculations are performed in the standard and advanced versions of the resonating group method. The standard version employs wave functions of the many-particle oscillator shell model to describe the internal motion of nucleons within each cluster. The advanced version is based on a three-cluster resonating group method. As in the standard version, the internal wave functions of three clusters are approximated by wave functions of the many-particle oscillator shell model. However, in the advanced version, a pair of clusters can form a bound state and then the third cluster is considered to interact with such two clusters, being in such the bound state. It is found that the Pauli resonance states in nuclei under consideration are observed at energies between 11 and 46 MeV, and their widths vary from 8 keV to 6.7 MeV. The analysis of the wave functions of Pauli resonance states and matrix elements of the norm kernel allowed us to formulate an effective method for eliminating Pauli resonance states. It is demonstrated that this method effectively eliminates all determined the Pauli resonance states.

DOI: [10.1103/PhysRevC.109.054614](https://doi.org/10.1103/PhysRevC.109.054614)

## I. INTRODUCTION

We study properties of the so-called Pauli resonance states which have been numerous observed in Refs. [1–12] and many others. These resonance states appear within the resonating group method (RGM) when one tries to use a more realistic description of interacting nuclei (clusters). They have been considered as redundant solutions of the equations of the resonating group method. As the Pauli resonance states appear not in all realizations (versions) of the resonating group method, we start with a short classification of main versions of the RGM, which are relevant to the subject of the present paper. The main difference of these methods is in the form of the wave function, which is used to approximate the cluster structure of a compound nucleus. The standard version of the RGM suggests the following form of the wave function of a two-cluster system of  $A$  nucleons for the partition  $A = A_1 + A_2$ :

$$\Psi(A) = \widehat{\mathcal{A}}\{\Phi_1(A_1, b)\Phi_2(A_2, b)\psi(\mathbf{x})\}, \quad (1)$$

where  $\mathbf{x}$  is a distance between centers of mass of clusters,  $\psi(\mathbf{x})$  is the wave function of the relative motion of clusters, and  $\Phi_1(A_1, b)$  and  $\Phi_2(A_2, b)$  are the wave functions of the many-particle oscillator shell model describing the motion

of nucleons within the first and second clusters, respectively. They are antisymmetric and translationally invariant. The oscillator length  $b$  determines the effective sizes of clusters. An important component of Eq. (1) is the antisymmetrization operator  $\widehat{\mathcal{A}}$  which makes the antisymmetric wave function of a compound system. For the sake of brevity, we omit all quantum numbers. They will be explicitly indicated in Sec. II.

In the second version, which we call the improved one, the wave function is chosen in the form

$$\Psi(A) = \widehat{\mathcal{A}}\{\Phi_1(A_1, b_1)\Phi_2(A_2, b_2)\psi(\mathbf{x})\}, \quad (2)$$

where different oscillator lengths  $b_1$  and  $b_2$  are used to improve the description of the internal structure of each cluster. This version is suitable for clusters with large difference of masses, i.e., for example, when  $A_1 \gg A_2$ .

The third version is called the advanced version of the RGM and related to the advanced description of the internal structure of one cluster,

$$\Psi(A) = \widehat{\mathcal{A}}\{\Phi_1(A_1, b_1)\Psi_2(A_2, b)\psi(\mathbf{x})\}. \quad (3)$$

Contrary to the wave function  $\Phi_\alpha(A_\alpha, b)$  ( $\alpha = 1, 2$ ), the wave function  $\Psi_\alpha(A_\alpha, b)$  is a solution of the two-cluster Schrödinger equation with clusterization  $A_\alpha = A_{\alpha 1} + A_{\alpha 2}$  and is presented in the form similar to (1). This version of the RGM suggests a more correct description of the compound system and is appropriate when one or both clusters  $A_1$  and  $A_2$  have an evident two-cluster structure, or, in other words, they have weakly bound state(s) and thus can be easily split

<sup>\*</sup>knurto1@gmail.com

<sup>†</sup>vsvasilevsky@gmail.com

into two fragments. Many light nuclei such as  $d$ ,  ${}^6\text{Li}$ ,  ${}^7\text{Li}$ , and  ${}^7\text{Be}$  have such properties as their separation energies are less than 3 MeV.

The Pauli resonance states have not been seen in the standard version of the RGM. Only the shape resonance states were detected within this version in the single-channel approximation. As is well known, the shape resonances are created by the centrifugal and/or Coulomb barriers. Thus, they lie relatively close to the threshold of the corresponding channel.

The Pauli resonance states have been detected in the improved and advanced versions of the RGM. The most spectacular demonstration of the Pauli resonance states was presented in Refs. [9,10], where the elastic scattering of  $\alpha$  particles on  ${}^{16}\text{O}$  has been calculated within the standard and improved versions. A set of narrow and wide resonance states emerged when different oscillator lengths (frequencies) were used for the wave functions describing the internal structure of  ${}^{16}\text{O}$  and  ${}^4\text{He}$  nuclei. They spread over a wide energy interval from small to relatively high energies above the  ${}^{16}\text{O} + {}^4\text{He}$  threshold. For example, in Ref. [9], in the  $0^+$  state, the improved version generates four resonance states with the energy less than 30 MeV, while the standard version creates no resonance states. These results have been obtained with the delta-shape nucleon-nucleon potential. In Ref. [10], the same models were used for the resonance structure in the  ${}^{16}\text{O} + {}^4\text{He}$  scattering, but with a semirealistic nucleon-nucleon potentials. It was found that, in this case, the Pauli resonances are shifted to the high-energy region ( $E > 30$  MeV).

In light nuclei, within the advanced version of the RGM [1–4,6–8,11], the Pauli resonance states have been observed in a relatively high-energy region  $E > 15$  MeV. It was also noticed in Ref. [2] that the Pauli resonance states manifest themselves in the states with small values of the total orbital momentum  $L$ .

Despite that the different authors have used different names for such type of resonances, such as “positive energy bound states” [1], “redundant” [5], or “spurious states” [7], it was widely recognized that the correctly treated Pauli principle is the origin of those states.

Why are the Pauli resonances considered as spurious states? There are two reasons for treating such resonance states. First, there are no physical justifications for the appearance of Pauli resonances. Second, such resonances are not observed experimentally.

To clarify the first reason, let us recall the main types of resonance states that are observed in many-particle and particular in nuclear systems (see, for example, Refs. [13–15]). The first type is shape resonance states which are created by centrifugal or/and Coulomb barriers. The second type is represented by the Feshbach resonance states [14,15]. These resonance states appear due to a weak coupling between open and closed channels. There are two necessary conditions for creating the Feshbach resonances. A compound system should have at least two channels with different threshold energies, and there should be at least one bound state in the channel with the larger threshold energy provided that this channel is considered separately from the channel with the lowest threshold energy.

The phenomenon which is called the Pauli resonance state cannot be explained by two main factors creating resonance states and, thus, cannot be attributed to the first or second type of resonances. It cannot be the Feshbach resonance as such resonance states observed in single-channel cases. It is impossible to relate the Pauli resonances to centrifugal or Coulomb barrier, since they appear in states with zero or very small angular momenta, or they require a very huge barrier.

To understand the phenomenon of Pauli resonance states, it is worth to recall some properties of the antisymmetrization operator  $\hat{A}$ . First, this operator been applied to a many-particle function that makes this function totally antisymmetric with respect to a permutation of any pair of particles or annihilates it. The latter means that such wave function cannot be antisymmetric. It is said that the Pauli principle prohibits such function or makes it forbidden. Usually, such type of functions describes many-particle systems, when more than four nucleons occupy the same single-particle orbital. Second, the antisymmetrization operator may significantly affect the normalization properties of many-particle functions. If the operator  $\hat{A}$  is applied to a wave function, which is normalized to unity, then the overlap of the resulting antisymmetric wave function can be smaller than unity, larger than unity, or even very small.

Both properties of the antisymmetrization operator  $\hat{A}$  have a great impact on the structure of equations for many-cluster systems and on the explicit form and the interpretation of obtained solutions. These properties are discussed in more detail in the following sections of the paper.

The Pauli resonance states have been considered as redundant solutions of the RGM equations. Thus, one needs to use an algorithm to eliminate these states. They distort real physical quantities such as the phase shifts, cross sections of various processes, and so on. To the best of our knowledge, there is only one algorithm for eliminating the Pauli resonance states. It was formulated in Ref. [12] and applied to the  ${}^4\text{He} + {}^{16}\text{O}$  system. We refer to this method as the REV method, which removes the eigenvalues of the norm kernel that cause the Pauli resonances. It was suggested in Ref. [12] to omit the so-called almost forbidden Pauli states. The criterion how to distinguish such states from allowed ones was formulated. This algorithm has eliminated all Pauli resonance states from the elastic scattering of  $\alpha$  particles on  ${}^{16}\text{O}$ .

In the present paper, we are going to examine the continuous-spectrum states of a set of light nuclei such as  ${}^6\text{Li}$ ,  ${}^7\text{Li}$ ,  ${}^7\text{Be}$ ,  ${}^8\text{Be}$ ,  ${}^9\text{Be}$ , and  ${}^{10}\text{B}$ . All these nuclei are considered as a three-cluster configuration and treated within a three-cluster model formulated in Ref. [16]. The three-cluster configuration is then reduced to three (if all three clusters are different) or two (if two of three clusters are identical) binary channels. When such reduction causes a pair of clusters to form a bound state, this state is described by the two-cluster approximation in our method.

To study the Pauli resonance states, we first analyze the overlap matrix and its eigenvalues for several light nuclei. Based on this analysis, we suggest an alternative method for eliminating the Pauli resonance states. We call this new method of removing of the oscillator functions the ROF method. We will demonstrate that both methods of REV and

ROF give close results and completely eliminate all Pauli resonance states.

The structure of the present paper is as follows. In Sec. II, we give a brief introduction of the methods applied to study properties of the Pauli resonances in light nuclei. In Sec. III, the choice of input parameters and the details of calculations are discussed. The manifestations of the Pauli resonance states in various two-cluster systems are demonstrated in Sec. III A. The analysis of the parameters of Pauli resonance states and their wave functions is carried out in this section. Then in the Sec. III E, we analyze the matrix elements and the eigenvalues of a norm kernel. In Sec. IV, we briefly explain the main idea of eliminating the Pauli resonance states suggested in Ref. [12]. Here we also demonstrate its efficiency. In Sec. V, we formulate an alternative method for eliminating the Pauli resonance states and demonstrate how it works in a two-cluster systems under consideration. Concluding remarks are presented in Sec. VI.

## II. METHOD

In this paper we will use two types of two-cluster functions and, thus, two realizations of the RGM. The first type of functions represents the standard form of the resonating group method, and the second type realizes the advanced form of the RGM. The wave function of the first type for a partition  $A = A_1 + A_2$  reads

$$\Psi_{E,J}(A) = \widehat{A}\{[\Phi_1(A_1, L_1, S_1, b)\Phi_2(A_2, L_2, S_2, b)]_S \times \psi_{E,I,L,J}(x)Y_I(\widehat{\mathbf{x}})]_L\}_J, \quad (4)$$

and the wave functions of the second type for the partition  $A = A_1 + A_2 = A_{21} + A_{22}$  are

$$\Psi_{E,J}(A) = \widehat{A}\{[\Phi_1(A_1, L_1, S_1, b)\Psi_2(A_2, L_2, S_2, b)]_S \times \psi_{E,I,J}(x)Y_I(\widehat{\mathbf{x}})]_L\}_J, \quad (5)$$

where  $\Psi_2(A_2, S_2, L_2, b)$  is the wave function of a bound state of the two-cluster subsystem with the partition  $(A_{21} + A_{22})$

$$\Psi_2(A_2, L_2, S_2, b) = \widehat{A}\{[\Phi_1(A_{21}, S_{21}, b)\Phi_2(A_{22}, S_{22}, b)]_{S_2} \times g_{E,\lambda,J}(y)Y_\lambda(\widehat{\mathbf{y}})]_J\}. \quad (6)$$

Recall that we use the capital letter  $\Phi$  to denote the wave functions that are not solutions of the corresponding Schrödinger equation, they are the wave functions of the many-particle oscillator shell model. These functions can be constructed as Slater determinants from single-particle oscillator orbitals. The capital and small letters  $\Psi$  and  $\psi$  represent solutions of the many-particle Schrödinger equation or corresponding integrodifferential Wheeler equation [17,18].

It is necessary to note that the many-particle shell model, employing the harmonic oscillator potential as a nucleon-nucleon interaction, provides an analytical and simple form of many-particle wave functions. These functions fairly well describe the low-energy spectra of light nuclei and many important parameters, such as charge root-mean-square radii, quadrupole momenta, and so on. They are widely used in different versions of the RGM. The coordinate part of these wave functions for  $s$ -shell nuclei ( $d$ ,  ${}^3\text{H}$ ,  ${}^3\text{He}$ , and  ${}^4\text{He}$ ) has

simple form

$$\Phi_\alpha(A_\alpha) \approx \exp\left\{-\frac{1}{2b^2} \sum_{1 \leq i < j}^{A_\alpha} (\mathbf{r}_i - \mathbf{r}_j)^2\right\},$$

where  $\mathbf{r}_i$  is a coordinate of  $i$ th particle. This form of cluster wave functions  $\Phi_\alpha(A_\alpha)$  allows one to obtain matrix elements of nucleon-nucleon interaction in a simple analytical form, provided that the nucleon-nucleon potential has a Gaussian form.

Here we use the  $LS$  coupling scheme, when the total spin  $S$  is a vector sum of spins of clusters, and the total orbital momentum  $L$  is a vector sum of the orbital momenta of both clusters  $L_1$  and  $L_2$  and the orbital moment of the relative motion of clusters  $l$ .

In the present paper, we consider the special case of the advanced version of the RGM. The usage of the special case is justified by employing the three-cluster model for investigating the cluster-cluster scattering and the structure of a compound nucleus. In this special case, only one of two functions  $\Psi_1$  and  $\Psi_2$  of the internal motion of nucleons is a solution of the two-cluster Schrödinger equation, and another function is the many-body oscillator shell-model wave function. A four-cluster model will allow one to consider the general case with two wave functions  $\Psi_1$  and  $\Psi_2$  to be solutions of the two-cluster Schrödinger equations.

To realize the advanced model, we employ the three-cluster model which was proposed in Refs. [16,19]. Within this model, a three-cluster configuration is transformed into a set of binary channels, i.e., in several pairs of interacting nuclei, and one of the interacting nuclei is considered as a two-cluster system. In Refs. [16,19], the model has been applied to study nuclei  ${}^7\text{Be}$  and  ${}^7\text{Li}$  with three-cluster configurations  ${}^4\text{He} + d + n$  and  ${}^4\text{He} + d + p$ , respectively. The structure of the  ${}^{10}\text{B}$  nucleus has been investigated in Ref. [20] by employing the three-cluster configuration  ${}^4\text{He} + {}^4\text{He} + d$ . Recently, the model which involves two three-cluster configurations  ${}^4\text{He} + p + n$  and  ${}^3\text{H} + d + p$  was used in Ref. [21] to study the resonance states of  ${}^6\text{Li}$  in a wide energy range.

The model involves the Gaussian basis functions to determine bound-state wave functions of two-cluster subsystems and the oscillator basis functions to describe the scattering of the third cluster on a bound state of the two-cluster subsystem. The abbreviation AMGOB is used to distinguish this model. In the AMGOB, two-cluster (6) and three-cluster (5) wave functions are represented as

$$\Psi_2(A_2, S_2, L_2, b) = \sum_{\nu=1}^{N_G} D_\nu^{E,L_2,J} \widehat{A}\{[\Phi_1(A_{21}, S_{21}, b) \times \Phi_2(A_{22}, S_{22}, b)]_{S_2} G_{L_2}(x, b_\nu) Y_{L_2}(\widehat{\mathbf{x}})]_J\}, \quad (7)$$

$$\Psi_{E,J}(A) = \sum_{n=0}^{N_O} C_{nL}^{E,J} \widehat{A}\{[\Phi_1(A_1, S_1, b)\Psi_2(A_2, S_2, L_2, b)]_{S,L_2} \times \Phi_{n,L}(y, b) Y_L(\widehat{\mathbf{y}})]_J\}, \quad (8)$$

where

$$G_L(x, b_v) = \frac{1}{b_v^{3/2}} \sqrt{\frac{2}{\Gamma(L+3/2)}} \rho^L \exp\left\{-\frac{1}{2}\rho^2\right\}, \quad \left(\rho = \frac{x}{b_v}\right), \quad (9)$$

is the Gaussian function and

$$\Phi_{n,L}(y, b) = (-1)^n \mathcal{N}_{nL} b^{-3/2} \rho^L e^{-\frac{1}{2}\rho^2} L_n^{L+1/2}(\rho^2),$$

$$\rho = \frac{y}{b}, \quad \mathcal{N}_{nL} = \sqrt{\frac{2\Gamma(n+1)}{\Gamma(n+L+3/2)}}, \quad (10)$$

is the oscillator function. In Eqs. (9) and (10),  $b_v$  and  $b$  denote oscillator lengths. The motivation to use these functions can be found in Ref. [16]. The expansion coefficients  $D_v^{E,L_2,J}$  and  $C_{nL}^{E,J}$  are solutions of a set of linear equations originated from the corresponding Schrödinger equations. This is a system of equations for the expansion coefficients  $D_v^{E,L_2,J}$ ,

$$\sum_{\tilde{v}=0} [G\langle v, L_2 | \hat{H}^{(2)} | \tilde{v}, L_2 \rangle_G - E_G \langle v, L_2 | \tilde{v}, L_2 \rangle_G] D_v^{E,L_2,J} = 0, \quad (11)$$

and we have a system of equations for the expansion coefficients  $C_{nL}^{E,J}$ :

$$\sum_{\tilde{n}=0} [\langle n, L | \hat{H} | \tilde{n}, L \rangle - E \langle n, L | \tilde{n}, L \rangle] C_{\tilde{n}L}^{E,J} = 0. \quad (12)$$

The system of Eqs. (11) involves matrix elements of the two-cluster Hamiltonian

$$G\langle v, L_2 | \hat{H}^{(2)} | \tilde{v}, L_2 \rangle_G$$

and the unit operator (norm kernel)  $G\langle v, L_2 | \tilde{v}, L_2 \rangle_G$  between cluster Gaussian functions

$$|v, L_2\rangle_G = \hat{\mathcal{A}}\{\Phi_1(A_{21}, S_{21}, b)\Phi_2(A_{22}, S_{22}, b)\}_{S_2}$$

$$\times G_{L_2}(x, b_v) Y_{L_2}(\hat{\mathbf{y}})_J. \quad (13)$$

while the system of Eqs. (12) involves matrix elements of the three-cluster Hamiltonian  $\langle n, L | \hat{H} | \tilde{n}, L \rangle$  and the unit operator  $\langle n, L | \tilde{n}, L \rangle$  between cluster oscillator functions,

$$|n, L\rangle = \hat{\mathcal{A}}\{\Phi_1(A_1, S_1, b)\Psi_2(A_2, S_2, L_2, b)\}_{S_1, L_2}$$

$$\times \Phi_{n,L}(y, b) Y_L(\hat{\mathbf{y}})_J. \quad (14)$$

We will also use another basis of cluster oscillator functions

$$|n, L\rangle_0 = \hat{\mathcal{A}}\{\Phi_1(A_1, S_1, b)\Phi_2(A_2, S_2, L_2, b)\}_{S_1, L_2}$$

$$\times \Phi_{n,L}(y, b) Y_L(\hat{\mathbf{y}})_J \quad (15)$$

to expand the wave functions of two-cluster systems in the standard version of the RGM (4). It is obvious that the wave functions  $|n, L\rangle_0$  are a partial case of wave functions  $|n, L\rangle$ , when the second cluster has the most compact shape.

As was pointed out in Introduction, the Pauli principle plays the paramount role in nuclear systems. The Pauli principle is realized through the antisymmetrization operator  $\hat{\mathcal{A}}$ . Two main properties of the operator were mentioned in Introduction. Now, we consider the second property—the action of the antisymmetrization operator on the normalization properties of wave functions. Consider, for example, the wave

functions (14) and (15). Each function in (14) and (15) to the right of the antisymmetrization operator is normalized to unity. However, the antisymmetric functions in the general case are not normalized to unity, as we shall see below. The overlap  $\langle n, L | n, L \rangle$  deviates from unity, when the quantum number  $n$  is small or, in other words, when the distance between clusters is small. The antisymmetrization operator makes the overlap  $\langle n, L | n, L \rangle$  larger than unity or smaller. In some cases, it makes  $\langle n, L | n, L \rangle$  very close to zero. Undoubtedly, these properties of the antisymmetrization operator have to be taken into account, when we are solving Eq. (12).

The appearance of the matrix  $\|\langle n, L | \tilde{n}, L \rangle\|$  in Eq. (12) indicates that the cluster oscillator basis (14) is not orthonormal, despite that all functions to the right of the antisymmetrization operator in Eq. (14) are normalized to unity on the corresponding part of the coordinate space. This matrix plays an important role in cluster models. It reflects effects of the Pauli principle. If one neglects the total antisymmetrization by putting  $\hat{\mathcal{A}} = 1$ , then one obtains the unit matrix  $\|\langle n, L | \tilde{n}, L \rangle\|$ . When the effects of the Pauli principle are small, then the diagonal matrix elements are close to unity, and the off-diagonal matrix elements tend to zero. Such behavior of the matrix elements  $\langle n, L | \tilde{n}, L \rangle$  is observed for large values of  $n$  and  $\tilde{n}$ . This region of quantum numbers  $n$  and  $\tilde{n}$  corresponds to large distances between clusters and, thus, is called the asymptotic region.

In the standard version of the RGM, the matrix  $\|\langle n, L | \tilde{n}, L \rangle\|$  is diagonal for two  $s$  clusters, as the orbital momenta of the first and second clusters  $L_1 = L_2 = 0$ . Within the advanced version of the RGM, as will be demonstrated below, the matrix  $\|\langle n, L | \tilde{n}, L \rangle\|$  is not diagonal. However, the largest matrix elements are situated on the main diagonal of the matrix.

It is worthwhile noticing that the wave functions  $\{C_{nL}^{E,J}\}$  obtained by solving the system of equations (12) are normalized by the conditions

$$\sum_{n, \tilde{n}=0} C_{nL}^{E,J} \langle n, L | \tilde{n}, L \rangle C_{\tilde{n}L}^{E,J} = \delta_{\alpha\beta} \quad (16)$$

for states of the discrete spectrum and

$$\sum_{n, \tilde{n}=0} C_{nL}^{E,J} \langle n, L | \tilde{n}, L \rangle C_{\tilde{n}L}^{\tilde{E},J} = \delta(E - \tilde{E}) \quad (17)$$

for the continuous-spectrum states. An important consequence of Eqs. (16) and (17) is that the value  $|C_{nL}^{E,J}|^2$  does not determine the contribution of the oscillator functions  $|n, L\rangle$  to the norm of a bound state or continuous-spectrum state.

To solve Eq. (12) for a finite number of basis functions ( $n = 0, 1, 2, \dots, N_O - 1$ ), one needs to analyze the  $N_O \times N_O$  matrix  $\|\langle n, L | \tilde{n}, L \rangle\|$ , whether this matrix contains redundant states which are called the Pauli forbidden states. For this aim, the diagonalization procedure is usually employed. It yields the eigenvalues  $\Lambda_\alpha$  ( $\alpha = 1, 2, \dots, N_O$ ) and corresponding eigenfunctions  $\|U_n^\alpha\|$  of the matrix  $\|\langle n, L | \tilde{n}, L \rangle\|$ . Eigenstates with  $\Lambda_\alpha = 0$  are called the Pauli forbidden states and have to be removed from the space. Eigenstates with small values of  $\Lambda_\alpha$  are called the partially or almost forbidden states. Usually, there are a large number of eigenstates with  $\Lambda_\alpha = 1$ . These



states are not affected by the antisymmetrization. Besides, the matrix  $\|\langle n, L|\hat{H}|\tilde{n}, L\rangle\|$  can have eigenvalues with  $\Lambda_\alpha > 1$ . They are called the super allowed states.

Note that the construction of the Pauli allowed states is a key problem for many-cluster systems. Many algorithms have been formulated (see, for example, Refs. [22–24],) to construct and to select Pauli allowed states.

Actually, we have two different discrete representations of the Schrödinger equation. The first representation is the oscillator basis representation and will be referred as the  $n$  representation. The second representation is formed by eigenvalues of the norm kernel matrix and will be referred as the  $\alpha$  representation. We recall that both representations are related by the orthogonal matrix  $\|U_n^\alpha\|$ .

In the  $\alpha$  representation, the set of Eq. (12) is transformed to the form

$$\sum_{\tilde{\alpha}=1}^{N_\alpha} [\langle \alpha, L|\hat{H}|\tilde{\alpha}, L\rangle - E \Lambda_\alpha \delta_{\alpha,\tilde{\alpha}}] C_{\tilde{\alpha}L}^{E,J} = 0, \quad (18)$$

where

$$\langle \alpha, L|\hat{H}|\tilde{\alpha}, L\rangle = \sum_{n,\tilde{n}=0}^{N_\alpha} U_n^\alpha \langle n, L|\hat{H}|\tilde{n}, L\rangle U_{\tilde{n}}^\alpha. \quad (19)$$

If the cluster system under consideration contains no the Pauli forbidden states, then one may use the set of Eqs. (12) or (18), both sets give the same spectrum, but different wave functions. One has to use the set of equations (18), when there are one or more the Pauli forbidden states.

To study effects of the Pauli principle, we will analyze the overlap matrix  $\|\langle n, L|\hat{H}|\tilde{n}, L\rangle\|$ . We will also analyze the eigenvalues and eigenfunctions of the matrix.

Few words about stages of solving the three-cluster problem. Before solving the three-body or three-cluster equations, one has to solve the two-body or two-cluster problem(s). The energies of bound states of a two-cluster subsystem determine threshold energies which are of great importance for implementing the proper boundary conditions for the three-cluster system. Thus, at the first stage, we have to find the spectrum and wave functions of the two-cluster subsystem by solving the generalized eigenvalue problem represented by Eq. (11). To optimize calculations with the Gaussian wave functions, we parametrize a set of widths  $b_\nu$  with parameters  $b_0$  and  $q$  as

$$b_\nu = b_0 q^{\nu-1}, \quad \nu = 1, \dots, N_G. \quad (20)$$

The parameters  $a_0$  and  $q$  are used as variational parameters to minimize the ground-state energy of the two-cluster subsystem. Such parametrization of the Gaussian functions has been used in Refs. [25,26] for calculations of the structure of light nuclei in many-cluster models. If we involve  $N_G$  Gaussian functions to describe the two-cluster subsystem, then we obtain  $N_G$  solutions of the system of equations (11). One of them is the ground state for the lowest orbital momentum or the lowest bound state for larger orbital momenta, and other solutions are excited pseudobound states of the nucleus represented by two-cluster configurations. In our analysis of the Pauli resonance states, we neglect all pseudobound states and account for only the ground state. Such restriction is

TABLE I. List of nuclei to be considered, their three-cluster configurations (3C), binary channels (BC), and input parameters of calculations: oscillator length  $b$  and exchange parameter  $u$  of the Minnesota potential [28].

Nucleus	3C	BC	$b$ , fm	$u$	Source
${}^6\text{Li}$	${}^4\text{He} + p + n$ ${}^3\text{H} + d + p$	${}^4\text{He} + d$ ${}^3\text{H} + {}^3\text{He}$	1.285	0.863	[21]
${}^7\text{Li}$	${}^4\text{He} + d + n$	${}^4\text{He} + {}^3\text{H}, {}^6\text{Li} + n$	1.311	0.956	[19]
${}^7\text{Be}$	${}^4\text{He} + d + p$	${}^4\text{He} + {}^3\text{He}, {}^6\text{Li} + p$	1.311	0.956	[16]
${}^8\text{Be}$	${}^4\text{He} + d + d$	${}^6\text{Li} + d$	1.311	0.956	
${}^9\text{Be}$	${}^4\text{He} + {}^3\text{H} + d$	${}^6\text{Li} + {}^3\text{H}$	1.285	0.950	[27]
${}^{10}\text{B}$	${}^4\text{He} + {}^4\text{He} + d$	${}^8\text{Be} + d, {}^6\text{Li} + {}^4\text{He}$	1.298	0.900	[20]

relevant to the physical reality for selected nuclei and makes our analysis more transparent.

At the second stage, we find the phase shift  $\delta_J$  of the scattering of the third cluster on the two-cluster subsystem by solving the system of linear equations (12) or (18).

Having determined the phase shifts  $\delta_J$  as functions of the energy  $E$ , we can determine the energy  $E_r$  and the total width  $\Gamma$  for an isolated resonance state from the equations

$$\left. \frac{d^2 \delta_J}{d^2 E} \right|_{E=E_r} = 0, \quad \Gamma = \left. \left( \frac{d \delta_J}{d E} \right)^{-1} \right|_{E=E_r}, \quad (21)$$

which utilize the well-known Breit-Wigner formula.

### III. RESULTS AND DISCUSSIONS

As was indicated above, we consider a set of light nuclei. In Table I, we list these nuclei and present details of the model and calculations. Here 3C denotes a three-cluster configuration which is taken into consideration, BC indicates binary channels which are studied. The Minnesota potential (MP) [28] is used as a nucleon-nucleon potential. The oscillator length  $b$  is chosen to minimize the energy of the three-cluster threshold. The exchange parameter  $u$  of the MP is usually selected to reproduce the ground-state energy of a compound system accounted from the lowest two- or three-body threshold.

For all nuclei (but not for  ${}^6\text{Li}$ ) listed in Table I, we employ only one three-cluster configuration. For  ${}^6\text{Li}$ , we employ two three-cluster configurations  ${}^4\text{He} + p + n$  and  ${}^3\text{H} + d + p$ . The first three-cluster configuration allows us to consider the dominant binary channel  ${}^4\text{He} + d$  and describe a deuteron as the  $p + n$  two-body system. The second three-cluster configuration is used to study the second binary channel  ${}^3\text{H} + {}^3\text{He}$  and to describe the nucleus  ${}^3\text{He}$  which is less bound than  ${}^3\text{H}$ , as the two-cluster structure  $d + p$ . We do not consider the alternative three-cluster configuration  ${}^3\text{He} + d + n$ , as the configuration  ${}^3\text{H} + d + p$  suggests a more realistic description of the  ${}^3\text{H} + {}^3\text{He}$  channel.

In the present paper, as was mentioned above, we employ the three-cluster model, which was designed to study the interaction of three  $s$  clusters. This allows us to study the scattering of  $s$ -shell clusters (such as  $n, d, {}^3\text{H}, {}^3\text{He}, {}^4\text{He}$ ) on  $s$ -shell clusters, and the scattering of  $s$ -shell clusters on

$p$ -shell clusters, such as  ${}^6\text{Li}$ ,  ${}^8\text{Be}$ . One can see from Table I, we selected clusters of  $s$ -shell and those  $p$ -shell clusters, which have zero value of the internal orbital momenta  $L_1 = L_2 = 0$  [see Eqs. (4) and (5)]. This selection substantially simplifies calculations and allows us to use the single-channel approximation. As the results, the total orbital momentum  $L$  coincides with the orbital momentum of relative motions of clusters. Besides, the spins  $S_1$  and  $S_2$  of the first and second clusters are good quantum numbers, even if the spin-orbit components of a nucleon-nucleon potential are involved.

We employ four Gaussian functions to obtain the energy and wave functions of two-cluster subsystems, and 100 oscillator functions to describe the scattering of the third cluster on the two-cluster subsystem. It was checked numerously that such number of oscillator functions is sufficient to obtain the bound-state energies of a compound nucleus and the scattering parameters with acceptable precision.

To consider properties of the Pauli resonances in more details, we restrict ourselves to the single-channel approximation. Moreover, we do not consider mixture of states with different values of the total orbital momentum  $L$  and total spin  $S$ , thus in our present model  $L$  and  $S$  are additional quantum numbers to the angular momentum  $J$  and parity  $\pi$  of a compound system. In this paper we will not consider many-channel cases. This is a subject for our next investigation.

#### A. Manifestation of the Pauli resonance states

In this subsection, we show how the Pauli resonance states manifest themselves in the continuous spectrum in the standard, improved and advanced versions of the RGM calculations. For this aim, we consider phase shifts. The most typical picture is shown in Fig. 1, where the phase shifts are displayed for two different  $J^\pi$  states of the elastic  ${}^4\text{He}+d$  and  ${}^3\text{He}+{}^3\text{H}$  scattering obtained with the  ${}^4\text{He}+p+n$  and  ${}^3\text{H}+d+p$  configurations, respectively. In Fig. 1 we display the phase shifts obtained in the advanced (A) and standard (S) versions of the RGM. As we can see, the phase shifts, obtained in the standard versions of the RGM, are monotonic functions of the energy, they do not exhibit the resonance behavior. Meanwhile, the phase shifts, in the advanced versions of the RGM, exhibit resonance states in the  $1^+$  ( $L=0$ ,  $S=1$ ) and  $2^-$  ( $L=1$ ,  $S=1$ ) states of  ${}^6\text{Li}$ . Note that at the low-energy region, the phase shifts obtained in the advanced (A) and standard (S) versions of the RGM are close one another. However, that is not the case for the phase shifts of the  ${}^4\text{He}+d$  scattering in the  $1^+$  states (i.e., in the state with  $L=0$ , and  $S=1$ ). Such a difference of the phase-shift behavior is determined by the position of the  ${}^6\text{Li}$  ground state in these two models. With the input parameters selected, the ground state is slightly bound in the advanced version, and in the standard version it is a pseudobound state. We recall that the wave functions of a deuteron and  ${}^3\text{He}$  are obtained in the two-cluster (two-body) approximations as  $p+n$  and  $d+p$ , respectively. Such advanced description of a deuteron and a triton stipulate the appearance of the Pauli resonance states shown in Fig. 1. Only one Pauli resonance state is found in each channel. The energies and widths of these resonances depend on the total orbital momentum  $J$ . One notices that there are two resonance

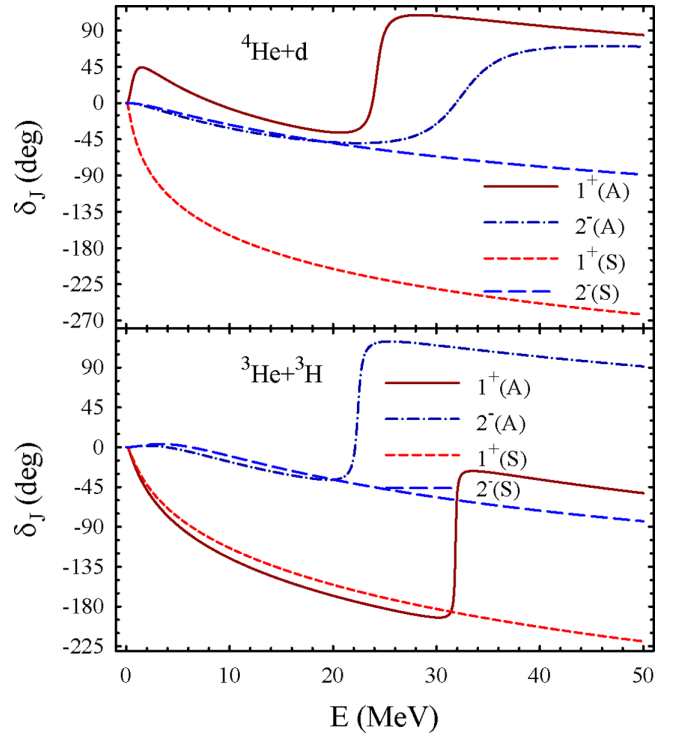


FIG. 1. Phase shifts of the elastic  ${}^4\text{He}+d$  and  ${}^3\text{He}+{}^3\text{H}$  calculated for the  $1^+$  and  $2^-$  states in the advanced version of RGM. Results are obtained with the standard (S) and advanced (A) versions of the RGM by using the  ${}^4\text{He}+p+n$  and  ${}^3\text{H}+d+n$  configurations, respectively.

states in the channel  ${}^4\text{He}+d$  with  $J^\pi = 1^+$ , and one of them is the Pauli resonance state with the energy  $E = 24.2$  MeV. The second one with the energy  $E = 0.257$  MeV and the width  $\Gamma = 0.226$  is the shape resonance state. The composition of the attractive nuclear and repulsive Coulomb interactions in the three-cluster system  ${}^4\text{He}+p+n$  created a favorable condition for creating the low-energy resonance. It is shown in Ref. [21] that this resonance state is transformed into the bound state in the four-channel approximation.

Another example of the Pauli resonance manifestation is shown in Fig. 2 for the  ${}^6\text{Li}+{}^4\text{He}$  scattering. This case demonstrates that the two-cluster system may have two Pauli resonance states; they are located at energy range  $10 \leq E \leq 45$  MeV. A sharp growing of the  $1^+$  phase shifts around 13.4 MeV indicates that there is very narrow resonance state with the widths  $\Gamma = 56$  keV. Other Pauli resonances are significantly wider.

Let us consider how the central part of the MP affects the energies and widths of the Pauli resonance states. This can be done by varying the exchange parameter  $u$  of that potential. This parameter affects the interaction of nucleons in odd states, as well as the cluster-cluster interaction. The smaller is  $u$ , the smaller is the interaction of clusters. When the parameter  $u$  approaches unity, the interaction of clusters increases. The influence of the parameter  $u$  variation is carried out for the  $3/2^-$  state of  ${}^7\text{Li}$  considered as two-cluster system  ${}^4\text{He}+{}^3\text{H}$ . Results of the variation of  $u$  are demonstrated for

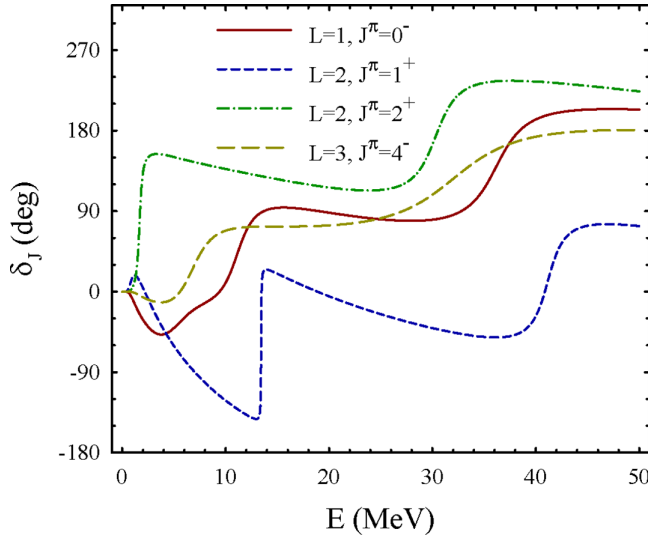


FIG. 2. Phase shifts of the elastic  ${}^6\text{Li} + {}^4\text{He}$  scattering as a function of the energy  $E$ . Results are obtained by the  ${}^4\text{He} + {}^4\text{He} + d$  calculation.

the ground-state energy  $E_{\text{GS}}$  and for the energy and width of the Pauli resonance. One can see in Fig. 3 that the parameter  $u$  changes the energy of the ground state. Moreover, when  $u < 0.86$ , the nucleus  ${}^7\text{Li}$  has no bound state. By varying the parameter  $u$  from 0.86 to 1, we change the ground-state energy from  $-0.038$  to  $-1.78$  MeV. However, the variation of

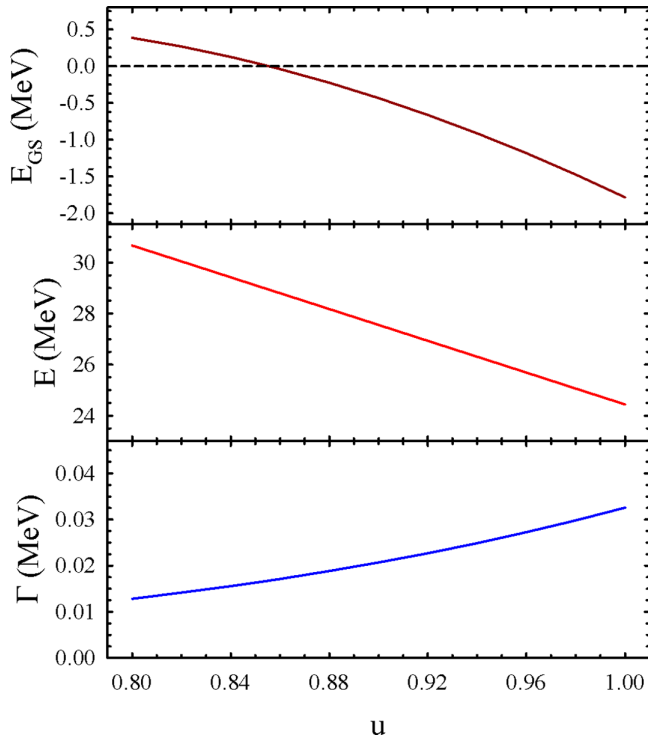


FIG. 3. Dependence of the ground-state energy  $E_{\text{GS}}$  of  ${}^7\text{Li}$ , the energy and width of the Pauli resonance state in the  $3/2^-$  state of the  ${}^4\text{He} + {}^3\text{H}$  channel on the exchange parameter  $u$  of the MP. Calculations are performed with the three-cluster configuration  ${}^4\text{He} + d + n$ .

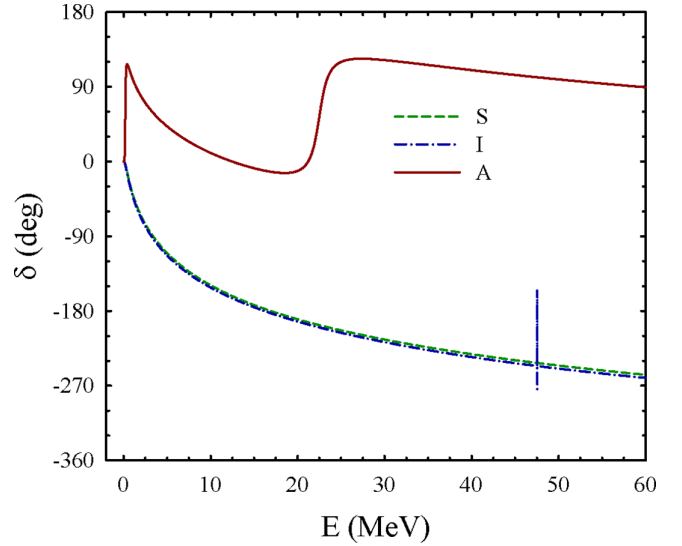


FIG. 4. Phase shifts of the elastic  ${}^4\text{He} + d$  scattering in the state  $L = 0, S = 1, J^\pi = 1^+$ , obtained in three different approximations of the RGM and with the  ${}^4\text{He} + p + n$  calculation.

$u$  from 0.8 to 1 reduces significantly the energy of the Pauli resonance from 30.67 to 24.44 MeV. Such a variation of  $u$  slightly changes the width of the Pauli resonance state from 13 to 33 keV.

Note an unusual feature of the Pauli resonance displayed in Fig. 3: The width of the resonance is decreasing with increasing of the exchange parameter  $u$ . For shape resonance states is usually observed another feature, both energy and width are decreasing with increasing of the parameter  $u$ .

### B. Special case for ${}^4\text{He} + d$ system

Taking into account peculiarities of our model, we decided to carry out an additional investigation of the  ${}^4\text{He} + d$  system. In this specific case, our model allows us to realize not only the standard and advanced, but also improved version of the RGM. If we take only one Gaussian function in the expansion of the deuteron wave function (i.e., to describe relative motion of a structureless proton and neutron) and select the parameters  $b_0$  [see Eqs. (7) and (20)] to minimize the bound-state energy of a deuteron, we realize therefore the improved version of the RGM. One Gaussian function with the optimal value of  $b_0 = 1.512$  fm creates a bound state of a deuteron with the energy  $E = -0.132$  MeV, while four Gaussian functions with optimal values of  $b_0$  and  $q$  [see Eq. (20)] generate the deuteron bound state with the energy  $E = -2.020$  MeV.

To locate the Pauli resonance state in the approximation in the energy region below 50 MeV, we have to change the exchange parameter  $u$  and take  $u = 1.0$ . In Fig. 4, we show the phase shift of the  ${}^4\text{He} + d$  scattering in the  $L = 0, S = 1, J^\pi = 1^+$  state obtained in three different approximations. The standard version of the RGM does not generate the Pauli resonance state in this case. The Pauli resonance states appear in the improved (I) and advanced (A) versions. The parameters of the Pauli resonance states substantially depend on the wave function describing the internal structure of a deuteron.

TABLE II. Parameters of the Pauli resonance states in  ${}^6\text{Li}$ ,  ${}^7\text{Li}$ , and  ${}^{10}\text{B}$ .

Nucleus	Channel	$L$	$S$	$J^\pi$	$E$ , MeV	$\Gamma$ , MeV
${}^6\text{Li}$	${}^4\text{He} + d$	0	1	$1^+$	24.218	1.165
		1	1	$2^-$	32.370	6.755
	${}^3\text{He} + {}^3\text{H}$	0	1	$1^+$	31.844	0.209
		1	1	$2^-$	22.403	0.618
${}^7\text{Li}$	${}^4\text{He} + {}^3\text{H}$	1	$1/2$	$1/2^-$	29.002	2.144
		1	$1/2$	$3/2^-$	25.810	0.027
		0	$1/2$	$1/2^+$	20.148	2.589
		0	$1/2$	$1/2^+$	34.444	4.702
	${}^6\text{Li} + n$	0	$1/2$	$1/2^+$	12.863	3.332
		0	$3/2$	$3/2^+$	18.895	0.196
${}^{10}\text{B}$	${}^6\text{Li} + {}^4\text{He}$	1	1	$0^-$	11.090	3.198
		1	1	$0^-$	35.834	4.600
		1	1	$1^-$	11.098	3.424
		1	1	$1^-$	36.167	5.105
		0	1	$1^+$	13.427	0.056
		0	1	$1^+$	41.144	2.751

A more realistic wave function significantly increases the width of the Pauli resonance (from  $\Gamma = 0.001$  MeV to  $\Gamma = 1.718$  MeV) and dramatically changes the energy (from  $E = 47.55$  MeV to  $E = 22.49$  MeV) of the resonance state in the state  $J^\pi = 1^+$ .

### C. Main properties of the Pauli resonance states

In Tables II and III we collect information on the parameters of Pauli resonance states detected in nuclei under consideration. Twenty-eight Pauli resonance states are detected. The energy of resonance states is reckoned from the threshold of the channel indicated in the column ‘‘Channel’’ of Tables II and III and varies from 11 to 46 MeV. There are 10 narrow resonance states with  $\Gamma < 1$  MeV, 6 of them are very narrow resonance states with the width  $\Gamma < 0.1$  MeV. The rest 18 resonance states are wider ones; their widths exceed 1

TABLE III. Energies and widths of the Pauli resonance states in  ${}^8\text{Be}$  and  ${}^9\text{Be}$  observed in the channels  ${}^6\text{Li} + d$  and  ${}^7\text{Li} + d$ , respectively.

Nucleus	Channel	$L$	$S$	$J^\pi$	$E$ , MeV	$\Gamma$ , MeV
${}^8\text{Be}$	${}^6\text{Li} + d$	0	0	$0^+$	17.233	3.553
		0	1	$1^+$	14.989	1.011
		0	1	$1^+$	25.724	4.628
		0	2	$2^+$	20.656	0.008
		1	0	$1^-$	18.253	0.058
		1	1	$2^-$	45.555	6.097
		1	1	$2^-$	18.523	0.008
		1	2	$3^-$	18.531	0.013
		1	2	$2^-$	20.981	0.402
		${}^9\text{Be}$	${}^7\text{Li} + d$	1	$1/2$	$1/2^-$
0	$1/2$			$1/2^+$	15.717	5.796
0	$1/2$			$1/2^+$	27.958	1.836

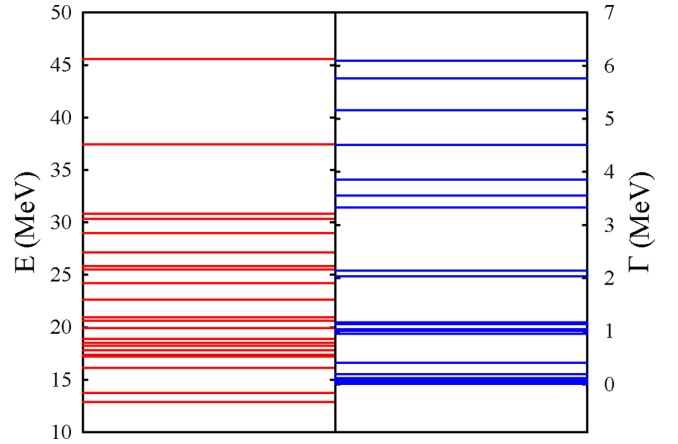


FIG. 5. Density of resonance state energies (left panel) and widths (right panel) of all determined Pauli resonance states.

MeV. One can see that, in most cases, the two-cluster system with fixed quantum numbers  $L$ ,  $S$ , and  $J^\pi$  has only one Pauli resonance state. However, there are some cases, where two Pauli resonance states are observed. The larger the energy of a resonance state, the larger is the total width. The energy of the second resonance state in  ${}^7\text{Li}$  and  ${}^8\text{Be}$  is approximately by 15 MeV larger than the energy of the first resonance state. In  ${}^{10}\text{B}$ , the energy difference is more than 25 MeV.

In Table III, we present the parameters of the Pauli resonance states obtained in different states for the  ${}^6\text{Li} + d$  and  ${}^7\text{Li} + d$  scattering.

By analyzing the results presented in Tables II and III, we came to the conclusion that the Pauli resonance states in light nuclei have energy more than 11 MeV, and their widths are mainly large ( $\Gamma > 0.9$  MeV). However, a few very narrow resonance states were found. The most populated area of resonance states lies in the interval  $16 < E < 21$  MeV, as it is demonstrated in Fig. 5 (left panel). Two dense area of widths of resonance states are located in the intervals  $0.008 < \Gamma < 0.22$  MeV and  $0.9 < \Gamma < 1.2$  MeV (Fig. 5, right panel). In many cases, only one Pauli resonance state appears in a binary channel. We also determined several cases with two resonance states.

In Fig. 6, we display the spectrum of Pauli resonances of positive-parity states with the total orbital momentum  $L = 0$ . These resonance states emerge in nuclei  ${}^7\text{Li}$ ,  ${}^8\text{Be}$ ,  ${}^9\text{Be}$ , and  ${}^{10}\text{B}$  with clusterization  ${}^6\text{Li} + A_2$ , where  $A_2$  denotes a neutron, deuteron, triton, and  $\alpha$  particle. This figure shows that the energies of the first Pauli resonance states are quite close for all nuclei. It also shows that there are two Pauli resonance states in the channel  ${}^6\text{Li} + d$  with the total spin  $S = 1$  and in the channel  ${}^6\text{Li} + {}^3\text{H}$  with the total spins  $S = 1/2$  and  $S = 3/2$ . One can see that the larger the second cluster, the larger is the energy of the highest Pauli resonance state. Indeed, it grows from 19 MeV in  ${}^6\text{Li} + n$  channel to 41 MeV in the channel  ${}^6\text{Li} + {}^4\text{He}$ .

The Pauli resonance states of negative parity created in the channel  ${}^6\text{Li} + A_2$  ( $A_2 = d, {}^3\text{H}, {}^4\text{He}$ ) with the total orbital momentum  $L = 1$  are shown in Fig. 7. We found no resonance state in the channel  ${}^6\text{Li} + n$ . In this channel, the Pauli



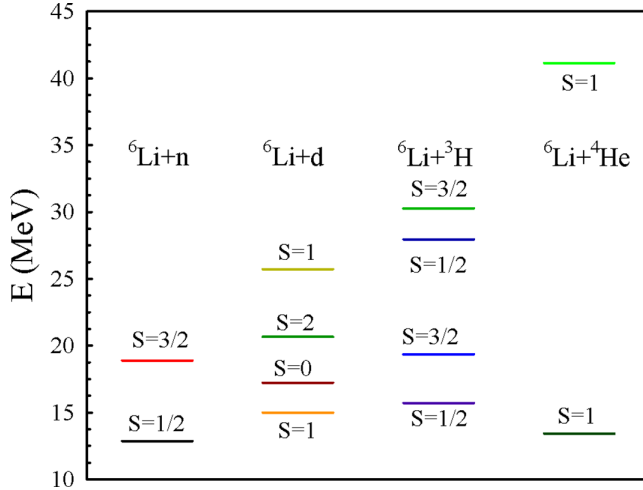


FIG. 6. Spectrum of positive-parity Pauli resonances for  $L = 0$  state of nuclei  ${}^7\text{Li}$ ,  ${}^8\text{Be}$ ,  ${}^9\text{Be}$ , and  ${}^{10}\text{B}$  detected in the channels  ${}^6\text{Li}+n$ ,  ${}^6\text{Li}+d$ ,  ${}^6\text{Li}+{}^3\text{H}$ , and  ${}^6\text{Li}+{}^4\text{He}$ , correspondingly.

resonance states do not appear neither in states with total spin  $S = 1/2$  nor in the states  $S = 3/2$ . Five Pauli resonance states are found in  ${}^8\text{Be}$  and  ${}^9\text{Be}$ , and four resonances are detected in  ${}^{10}\text{B}$ . Figure 7 shows that the energy of the lowest Pauli resonance state decreases, as the mass of the “projectile”  $A_2$  increases. It is an interesting tendency, as the Coulomb repulsion between  ${}^6\text{Li}$  and  $A_2$  increases with the mass of the second cluster  $A_2$ . It is necessary to underline that the spin-orbit interaction plays an important role in the formation of the Pauli resonance states.

To detect the Pauli and shape resonance states, we analyzed the behavior of phase shifts as functions of the energy. The rapid growth of the phase shift was considered as the signal of a resonance state. There is another way for detecting the resonance states of both types. This way is applicable for any method which involves a square integrable basis of func-

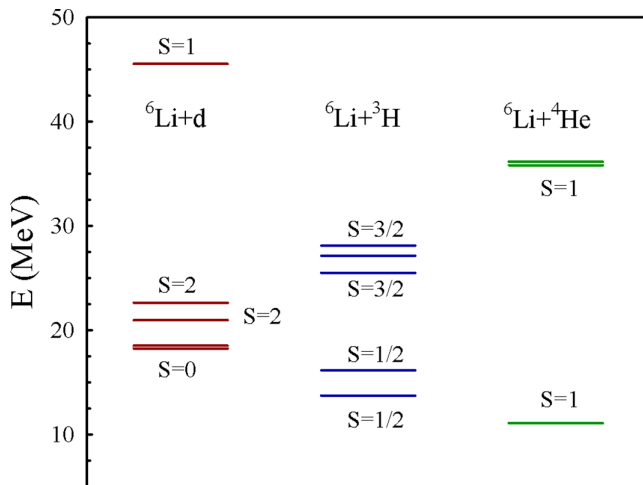


FIG. 7. Spectrum of the Pauli resonance states of the negative parity in  ${}^8\text{Be}$ ,  ${}^9\text{Be}$ , and  ${}^{10}\text{B}$  created in the state with the total orbital momentum  $L = 1$ .

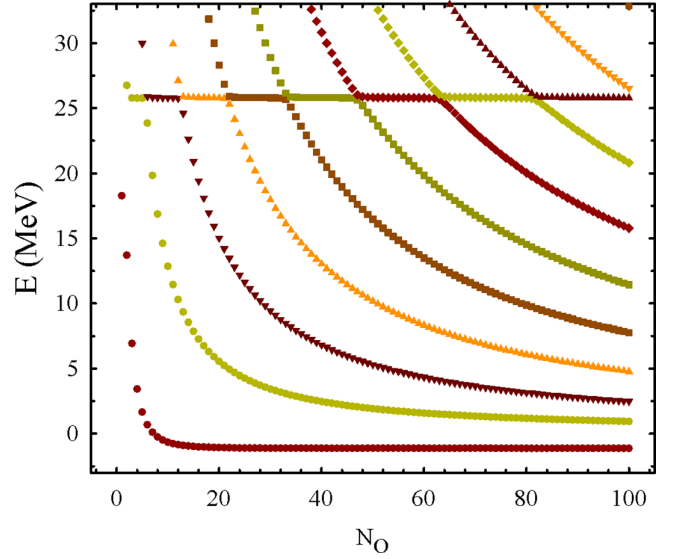


FIG. 8. Spectrum of the  $3/2^-$  states in  ${}^7\text{Li}$  as a function of the number of oscillator functions  $N_0$  involved in calculations. Calculations are performed with the three-cluster configuration  ${}^4\text{He}+d+n$ .

tions. Unfortunately, this method works for relatively narrow resonance states. The narrow resonance states can be detected by calculating the eigenenergies of a Hamiltonian with different numbers of basis functions. By displaying the eigenenergies as functions of the number of basis functions (we denote them as  $N_0$ ) involved in calculations, a resonance state will display itself as a plateau or/and as an avoid crossing. The energy of a plateau is the energy of a resonance state. Such way of detecting the resonance states is an essential element of the stabilization method (Ref. [29]) and the complex scaling method (see definitions of the method and its recent progress in applications to many-cluster systems in Refs. [30–32]).

In Fig. 8, we show the dependence of the eigenenergies of the  $3/2^-$  state in  ${}^7\text{Li} = {}^4\text{He} + {}^3\text{H}$  on the number of oscillator functions  $N_0$  used in calculations. We gradually change the number of oscillator functions from 1 to 100. One can see that it is necessary to use at least three oscillator functions to create a plateau or, in other words, to obtain the eigenvalue with the energy which is very close to the energy of a resonance state. Such a plateau unambiguously indicates the presence of a narrow resonance state. This result is naturally consistent with the results of phase-shift calculations. Besides, the wave functions of the resonance states obtained with 5, 10, and 100 oscillator functions are very close to one another in the region of small values of  $n$ , as it demonstrated in Fig. 9. It proves that the wave function of the narrow  $3/2^-$  resonance state is formed by oscillator functions with very small values of  $n$ .

#### D. Peculiarities of the Pauli resonance states

Let us consider peculiarities of the wave functions of Pauli resonance state. The analysis of wave functions will allow us to understand the nature of the Pauli resonances. The wave functions of resonant and nonresonant states are considered in the oscillator and coordinate representations.

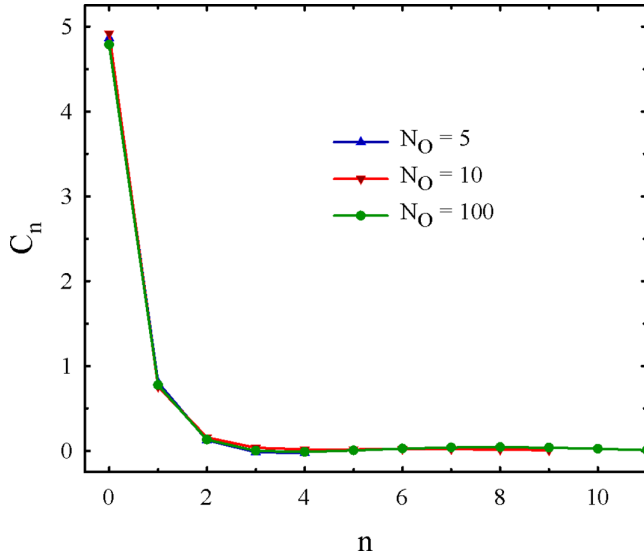


FIG. 9. Convergence of the wave function of the narrow  $3/2^-$  Pauli resonance state in  ${}^7\text{Li}$  in the channel  ${}^4\text{He} + {}^3\text{H}$ . Calculations are performed with the three-cluster configuration  ${}^4\text{He} + d + n$ .

In Fig. 10, we show three wave functions of the  $3/2^-$  states in  ${}^7\text{Li}$  for the clusterization  ${}^4\text{He} + {}^3\text{H}$ . One of these functions is the wave function of the ground state (GS), the second function is the Pauli resonance state (PR) with the energy  $E = 25.810$  MeV, and the third function is the wave function of the nonresonant elastic  ${}^4\text{He} + {}^3\text{H}$  scattering state (SS) ( $E = 10.1$  MeV). The main difference between the the wave functions of Pauli resonant and nonresonant states is the contribution of the oscillator function with  $n = 0$ . This function gives the largest contribution to the wave function of the Pauli resonance states, and it has the smallest contribution

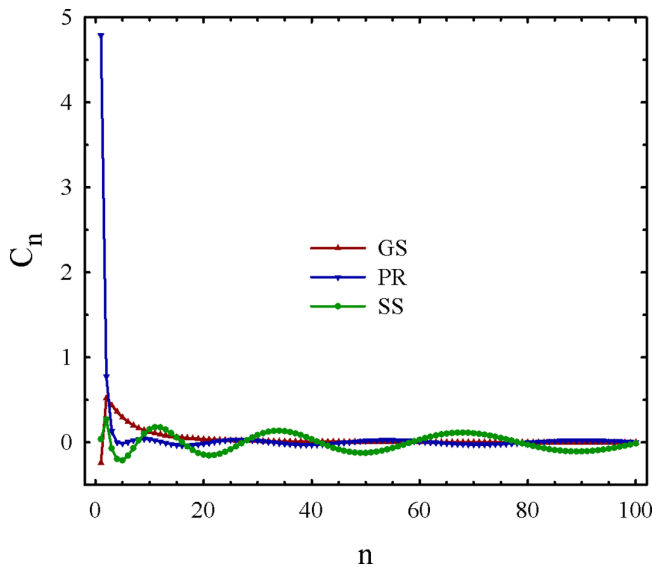


FIG. 10. Wave functions in the oscillator representation of the ground state (GS), Pauli resonance state (PR), and scattering state (SS) in the  $3/2^-$  state of  ${}^7\text{Li}$ . Results are obtained with the  ${}^4\text{He} + d + n$  calculations.

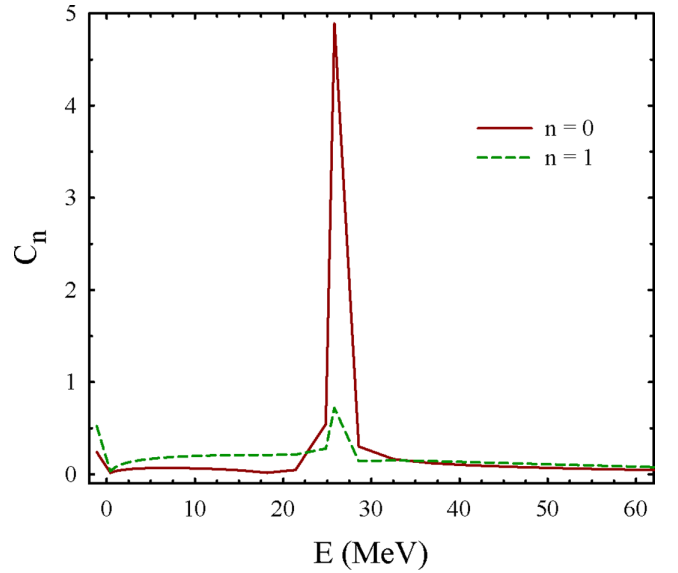


FIG. 11. Contribution of the oscillator wave functions with  $n = 0$  and  $n = 1$  to the wave functions of the continuous-spectrum  $3/2^-$  states of the  ${}^4\text{He} + {}^3\text{H}$  channel.

to the wave functions of the ground and continuous-spectrum states.

Figure 11 shows the general picture of the contribution of oscillator functions with the quantum numbers  $n = 0$  and  $n = 1$  to the wave functions of continuous-spectrum states over a large energy region. Figure 11 confirms also that the oscillator wave function with  $n = 0$  contribute mainly to the Pauli resonance state and gives a small contribution to other states of the  ${}^4\text{He} + {}^3\text{H}$  continuous spectrum.

### E. Overlap

As it was widely recognized that the Pauli resonance states appear due to the Pauli principle, it is then expedient to analyze its effects on the norm kernels. Matrix of the norm kernel in general case (for the improved and advanced versions of the RGM) is nondiagonal. Thus, we start the analysis with a 3D picture of the matrix. In Fig. 12, we display the overlap matrix  $\|\langle n|m\rangle\|$  for the channel  ${}^4\text{He} + {}^3\text{H}$  in the state  $L = 0$ ,  $S = 1/2$ , and  $J^\pi = 1/2^+$ . One can see that this matrix is a quasideagonal. The largest matrix elements are located on the main diagonal, and the larger is  $m = n$ , the closer they are to unity. Off-diagonal matrix elements  $\langle n|m\rangle$  are very small. A few diagonal matrix elements with small values of  $n$  are also small due to the Pauli principle. One may conclude that the Pauli principle has a short-range nature, since it affects a relatively small number of cluster basis functions  $|n\rangle$  determined in Eq. (14), and the corresponding matrix elements  $\langle n|m\rangle$ . Note that Fig. 12 demonstrates a typical behavior of the matrix elements of a norm kernel in the advanced version of the RGM for all nuclei and all states considered in this paper.

Figure 12 prompts us to study only the diagonal matrix elements of the norm kernel, which completely reflects effects of the Pauli principle. Consequently, in this subsection, we

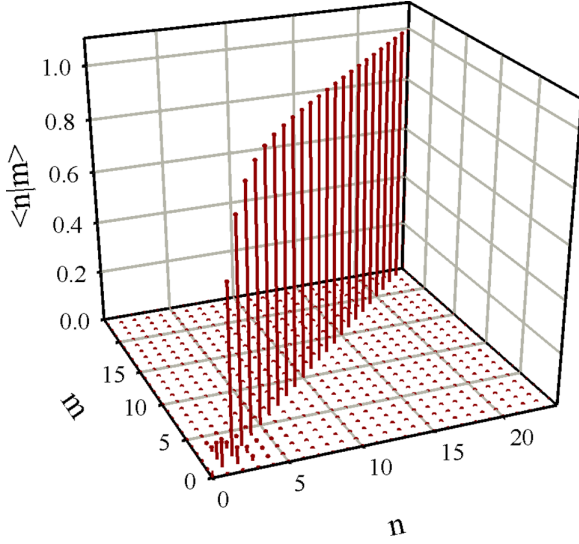


FIG. 12. Matrix for the norm kernel in the state  $L = 0$ ,  $S = 1/2$ , and  $J^\pi = 1/2^+$  of the channel  ${}^4\text{He} + {}^3\text{H}$ . Results are obtained with the  ${}^4\text{He} + d + n$  configuration.

discuss the diagonal matrix elements and eigenvalues of the norm kernel. In Fig. 13, we compare the diagonal matrix elements of the norm kernel determined in the standard (S) and advanced (A) versions of the RGM, for  ${}^7\text{Li}$  as a two-cluster configuration  ${}^4\text{He} + {}^3\text{H}$ . It is worth to recall that, in the standard version, the matrix of the norm kernel is diagonal. This figure demonstrates general features of the quantities  $\langle n|n\rangle$  and  $\Lambda_\alpha$  for all two-cluster systems under consideration. As was pointed out in the previous paragraph, the major part of diagonal matrix elements is equal to unity and only a small fraction of them differs from unity by showing effects of the Pauli principle. It is necessary to recall that the oscillator wave functions with small values of the quantum number  $n$  describe two clusters at the smallest relative distance. Thus, effects of the Pauli principle for these functions are prominent. One can see that there are two Pauli forbidden states in the  $1/2^+$  state and one in the  $3/2^-$  state within the standard version for  ${}^4\text{He} + {}^3\text{H}$ . In the advanced version, these basis states, namely  $|n, L\rangle = |0, 0\rangle$  and  $|1, 0\rangle$  for  $1/2^+$  and  $|0, 1\rangle$  for  $3/2^-$ , can be considered as almost forbidden Pauli states, since the corresponding diagonal matrix elements are very small ( $\langle n|n\rangle < 0.1$ ). Figure 13 demonstrates the important features of matrix elements: The number of forbidden states in the standard version coincides with the number of almost forbidden states in the advanced version.

In Fig. 14 we display the diagonal matrix elements  $\langle n|n\rangle$  and eigenvalues  $\Lambda_\alpha$  of the norm kernel for the  $0^+$  states of the advanced  ${}^6\text{Li} + d$  cluster system. Diagonal matrix elements also show that there are a few almost forbidden states when  $\langle n|n\rangle$  are close to zero. One may observe a set of the superallowed Pauli states ( $\langle n|n\rangle > 1$ ) for the total spin  $S = 1$  and  $S = 2$ . There are similarities between eigenvalues and the diagonal matrix elements of the norm kernel. The eigenvalues  $\Lambda_\alpha$  reveals a few almost forbidden states, two states for  $S = 1$  and one state for the total spin  $S = 0$  and  $S = 2$ . Similarly to

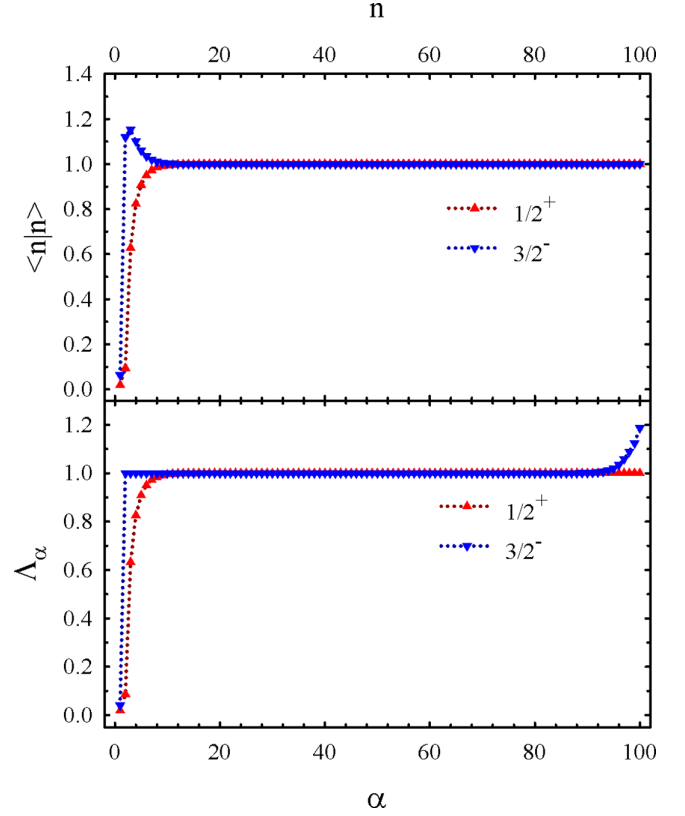


FIG. 13. Comparison of diagonal matrix elements of the norm kernel determined in the standard (S) and advanced (A) versions of the RGM for  $1/2^+$  and  $3/2^-$  states of  ${}^7\text{Li} = {}^4\text{He} + {}^3\text{H}$ . Results are obtained with the  ${}^4\text{He} + d + n$  configuration.

the diagonal matrix elements, the eigenvalues for  $S = 0$  and  $S = 2$  possess the superallowed states.

Diagonal matrix elements  $\langle n|n\rangle$  of the norm kernel and its eigenvalues  $\Lambda_\alpha$  for the channel  ${}^6\text{Li} + {}^4\text{He}$  in the advanced two-cluster system are displayed in Fig. 15. Two almost forbidden states are demonstrated by both diagonal matrix elements and eigenvalues. They are observed in two states:  $L = 0$ ,  $S = 1$ ,  $J^\pi = 1^+$  and  $L = 1$ ,  $S = 1$ ,  $J^\pi = 1^-$ .

Finishing this subsection, we conclude that the number of almost forbidden states coincides with the number of almost forbidden eigenstates. Almost forbidden states  $|n\rangle$  obey the restriction  $\langle n|n\rangle < 0.3$ , while almost forbidden eigenstates have  $\Lambda_\alpha < 0.2$ . Comparing the results demonstrated in Figs. 12–14 with the results in Tables II and III, we came to the conclusion that the number of almost forbidden states equals of the number of the Pauli resonance states.

#### IV. METHOD REV

Let us consider the main ideas of the REV method formulated in Ref. [12]. The authors of Ref. [12] paid attention to a set of eigenstates of the norm kernel appeared in the case when different oscillator lengths were used for an  $\alpha$  particle ( $b_\alpha = 1.395$  fm) and  ${}^{16}\text{O}$  ( $b_O = 1.776$  fm). These eigenstates have very small values as compared to eigenstates with the common oscillator length. For example, the smallest

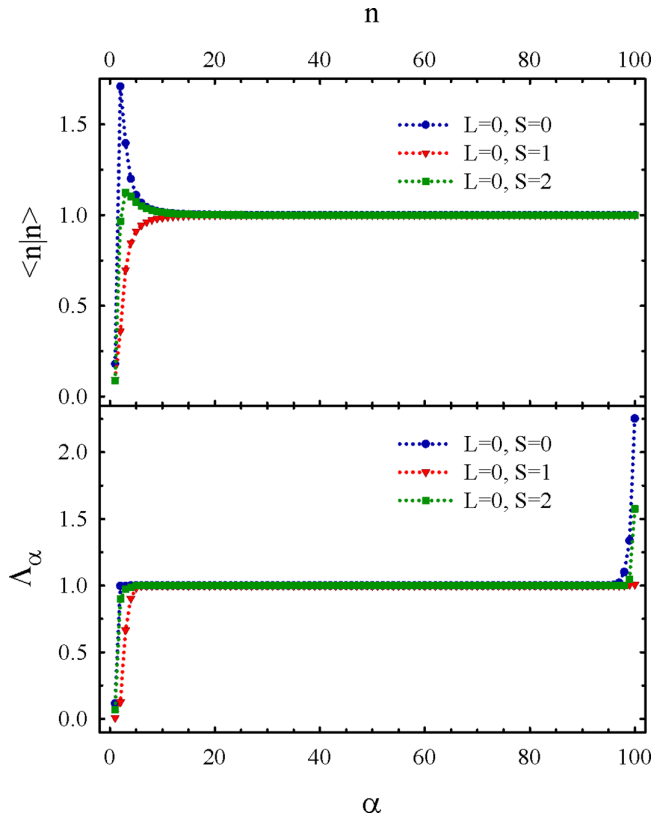


FIG. 14. Diagonal matrix elements (the upper panel) and eigenvalues (the lower panel) of the norm kernel for the  $L^\pi = 0^+$  states and different values of the total spin  $S$  in the two-cluster system  ${}^6\text{Li} + d$ . Results are obtained with the  ${}^4\text{He} + d + d$  model space.

eigenvalue is 0.229 for Pauli allowed positive-parity states in the standard version with the common oscillator length, while there are four eigenstates with eigenvalues less than 0.03 in the improved version with different oscillator lengths. The similar picture was also observed for the odd-parity states. The lowest eigenvalue is 0.344 for Pauli allowed states in the standard version. In the advanced version, four eigenstates emerge with eigenvalues less than 0.04.

It was suggested in Ref. [12] to eliminate such eigenvalues and to use a smaller set of norm kernel eigenstates. Thus, in the case of different oscillator lengths, all eigenstates with eigenvalues smaller than the smallest eigenvalue with the common oscillator length were treated as the Pauli forbidden states. Actually, the border between the Pauli allowed and Pauli forbidden states in system  ${}^4\text{He} + {}^{16}\text{O}$  was selected to be 0.1. Having applied such restrictions, all Pauli resonance states disappeared.

We will use this method to eliminate the Pauli resonance states which appear in light nuclei within the advanced resonating group method. The analysis of the eigenvalues of the norm kernel carried out in Sec. III E indicates that we have to redetermine the border between the Pauli allowed and Pauli forbidden states.

The efficiency of the REV method will be demonstrated in Sec. V A.

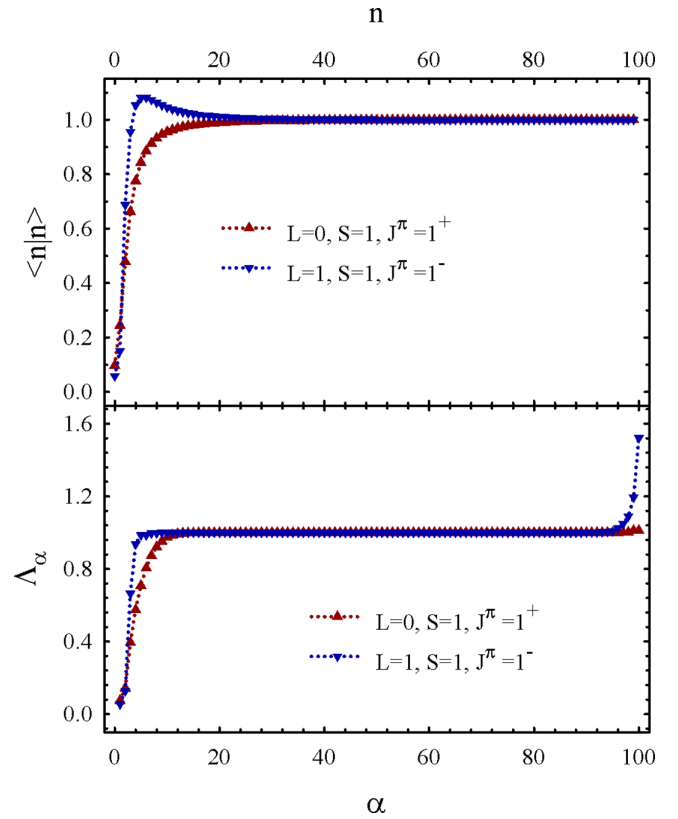


FIG. 15. Diagonal matrix elements (upper panel) and eigenvalues (lower panel) of the norm kernel for the channel  ${}^6\text{Li} + {}^4\text{He}$  in the states  $L = 0, S = 1, J^\pi = 1^+$  and  $L = 1, S = 1, J^\pi = 1^-$ . Results are obtained with the  ${}^4\text{He} + {}^4\text{He} + d$  model space.

## V. METHOD ROF

We suggest another method to struggle with the Pauli resonance states in light nuclei in the improved and advanced RGM calculations. This is because the Pauli resonances do not appear in actual nuclei but appear in theoretical calculations. The method is based on properties of the matrix elements of the norm kernel. By analyzing the properties of matrix elements, our attention was focused on the behavior of diagonal matrix elements  $\langle n|n \rangle$ . In many cases, the matrix element  $\langle 0|0 \rangle$  and, sometimes, matrix element  $\langle 1|1 \rangle$  are very small with respect to other diagonal matrix elements. The analysis also revealed that the matrix elements of the corresponding rows ( $\langle 0|n \rangle, \langle 1|n \rangle$ ) and columns ( $\langle n|0 \rangle, \langle n|1 \rangle$ ) are also very small. Besides, it was shown above (Sec. III D) that the oscillator functions with  $n = 0$  and, sometimes, with  $n = 1$  dominate in the wave functions of the Pauli resonance states. Thus, we suggest to omit those parts of the matrix  $\|\langle n|\tilde{n} \rangle\|$  whose diagonal matrix elements are very small. We also suggest a criterion of smallness for the diagonal matrix elements. Let us introduce the minimal value of the diagonal matrix elements  $O_{\min}$  which will mark a border between the Pauli forbidden (or almost forbidden) and Pauli allowed states. Within our method, all diagonal matrix elements which are smaller than  $O_{\min}$  will be omitted with their correspondent rows and columns.



The analysis of the diagonal matrix elements of the norm kernel leads us to the conclusion that in many improved and advanced two-cluster cases, considered above,  $O_{\min}$  can be set to 0.2. This can be seen in Figs. 14 and 15. Such a value can be also used both for the case of one or two Pauli resonance states.

It is important to notice that from mathematical point of view almost forbidden basis states or eigenstates are allowed states and should not create any problems. The same is true also from computational point of view, as the smallest eigenvalues are much larger than the smallest numerical value (numerical zero) in modern computers. Indeed, almost forbidden states do not create any problem for bound states and their parameters, such as root-mean-square mass and proton radii and so on. Presence of almost forbidden states affects (distorts) only continuous-spectrum states. In this respect, the REF and ROF methods suggest the redetermination of essentially allowed Pauli states. The REF and ROF methods determine border between almost forbidden and allowed states. This border is marked by  $\Lambda_{\min}$  and  $O_{\min}$  in the REF and ROF methods, respectively. In the general case, one can use  $\Lambda_{\min}$  and  $O_{\min}$  as variational parameters to control the number of eliminated basis states  $|n\rangle$  or eigenstates  $|\alpha\rangle$  and their effects on scattering parameters. Naturally, the main aim of such a procedure is to eliminate the Pauli resonance state(s) and to cause minimal effects on bound states and shape resonance states.

### A. Demonstration of the REV and ROF methods

Having analyzed the diagonal matrix elements and eigenvalues of the overlap matrix, we deduced  $O_{\min}$  and  $\Lambda_{\min}$  for all improved and advanced RGM calculations and for those states  $J^\pi$  which have the Pauli resonance states. These quantities are displayed in Table IV. In this table, we also indicated the number  $N_{f.s.}$  of eliminated basis functions or eigenfunctions.

In Fig. 16, we demonstrate efficiency of the REV and ROF methods for the  ${}^4\text{He} + {}^3\text{H}$  scattering in the  $1/2^+$  state. Here OA denotes the ordinary algorithm of obtaining phase shifts within the advanced version of the RGM. The phase shift in this approach exhibits two Pauli resonance states, parameter of which are shown in Table II and III. As we can see, both methods remove the Pauli resonance states. They also yield the phase shifts which are close to the standard version at low-energy region  $0 \leq E < 6$  MeV. There is very small difference of phase shifts obtained with the REV and ROF methods. We used minimal values of  $\Lambda_{\min} = O_{\min} = 0.2$ . This restriction eliminated two functions in both methods.

The similar picture is observed for the  ${}^4\text{He} + d$  scattering in the  $2^-$  state, see Fig. 17. Only one Pauli resonance state is generated in this case. Both REV and ROF methods remove that Pauli resonance state and produce the phase shifts with very small differences. In this case, we also used minimal values of  $\Lambda_{\min} = O_{\min} = 0.2$ . This restriction eliminated only one function in both methods.

Phase shifts of the elastic  ${}^6\text{Li} + d$  scattering obtained within three different approaches are shown in Fig. 18. As one can see, in this case, we observe both low-energy shape and high-energy Pauli resonance states. The REV and ROF methods

TABLE IV. Actual values of  $O_{\min}$  and  $\Lambda_{\min}$ , and the number of forbidden states  $N_{f.s.}$ , which are omitted to eliminate the Pauli resonance states.

Nucleus	Clusterization	$L$	$S$	$J^\pi$	$O_{\min}$	$\Lambda_{\min}$	$N_{f.s.}$
${}^6\text{Li}$	${}^4\text{He} + d$	0	1	$1^+$	0.2	0.2	1
		1	1	$2^-$	0.2	0.2	1
	${}^3\text{H} + {}^3\text{He}$	0	1	$1^+$	0.1	0.1	1
		1	1	$2^-$	0.1	0.1	1
${}^7\text{Li}$	${}^4\text{He} + {}^3\text{H}$	1	$1/2$	$3/2^-$	0.1	0.1	1
		1	$1/2$	$1/2^-$	0.1	0.1	1
		0	$1/2$	$1/2^+$	0.1	0.1	2
		2	$1/2$	$3/2^+$	0.1	0.1	1
	${}^6\text{Li} + n$	0	$1/2$	$1/2^+$	0.3	0.3	1
${}^8\text{Be}$	${}^6\text{Li} + d$	0	0	$0^+$	0.2	0.2	1
		0	1	$1^+$	0.1	0.1	1
		1	0	$1^-$	0.2	0.2	1
		1	1	$2^-$	0.3	0.3	1
		0	2	$2^+$	0.1	0.1	1
${}^9\text{Be}$	${}^6\text{Li} + {}^3\text{H}$	0	$1/2$	$1/2^+$	0.2	0.1	2
		1	$1/2$	$1/2^-$	0.1	0.1	1
		0	$3/2$	$3/2^+$	0.2	0.1	2
		1	$3/2$	$5/2^-$	0.1	0.1	1
		1	$3/2$	$5/2^-$	0.2	0.2	1
${}^{10}\text{B}$	${}^6\text{Li} + {}^4\text{He}$	1	1	$0^-$	0.3	0.2	2
		1	1	$1^-$	0.3	0.2	2
		2	1	$1^+$	0.2	0.2	2
		2	1	$2^+$	0.2	0.2	1
		2	1	$3^+$	0.2	0.2	1

eliminating one eigenfunction and one oscillator function, respectively, remove the Pauli resonance state. They also slightly change parameters of the shape resonance. In the

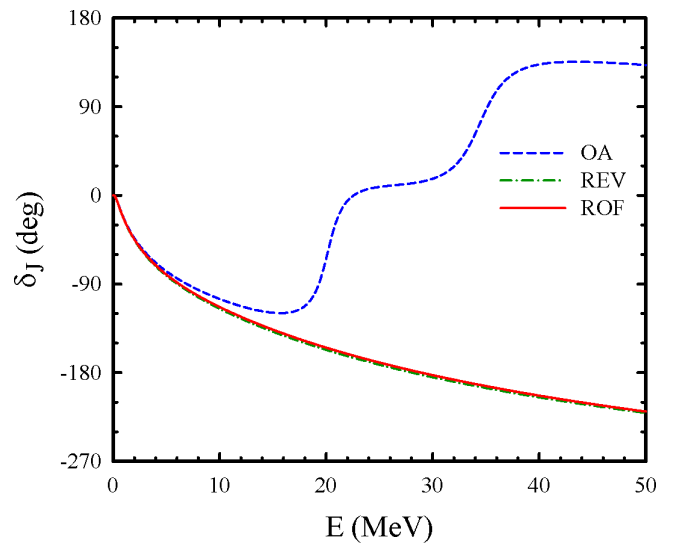


FIG. 16. Phase shifts of the elastic  ${}^4\text{He} + {}^3\text{H}$  scattering in the  $1/2^+$  state as a function of the energy determined in three different approaches. The three-cluster configuration  ${}^4\text{He} + d + n$  is involved in calculations.

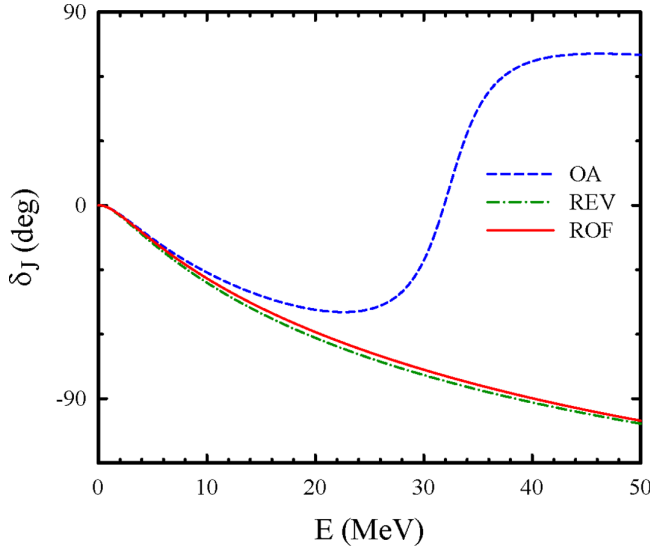


FIG. 17. Phase shifts of the elastic  ${}^4\text{He}+d$  scattering in the  $2^-$  state determined in three different approaches with the three-cluster configuration  ${}^4\text{He}+p+n$ .

OA, parameters of the shape resonance are  $E = 0.153$  MeV and  $\Gamma = 0.013$  MeV, while in the REV method they are  $E = 0.374$  MeV and  $\Gamma = 0.485$  MeV and, in the ROF method, we obtained  $E = 0.352$  MeV and  $\Gamma = 0.371$  MeV. Note that the REV and ROF give almost identical phase shifts for the  ${}^6\text{Li}+d$  scattering. This means that the eliminated eigenfunction of the norm kernel and the eliminated oscillator function are close to each other.

We found several cases where the REV and ROF methods give noticeable different phase shifts. One of such examples is shown in Fig. 19, where phase shifts of the  ${}^6\text{Li}+{}^4\text{He}$  scattering in the state  $L = 1, S = 1$ , and  $J^\pi = 1^-$  are drawn. Note that almost the same results are observed for the state

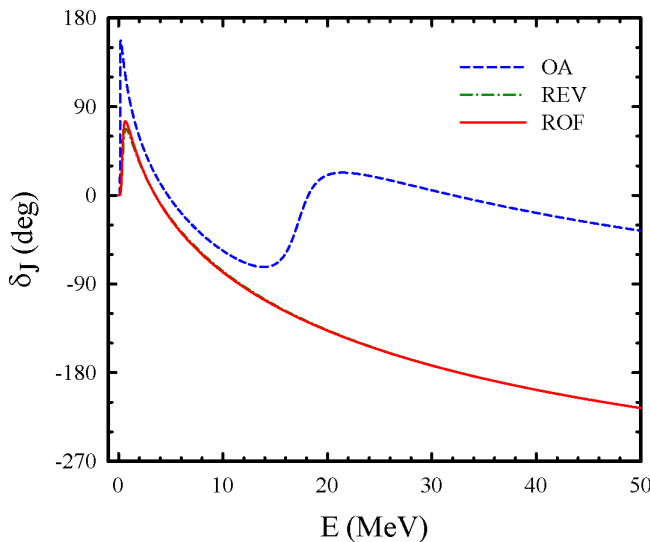


FIG. 18. Phase shifts of the elastic  ${}^6\text{Li}+d$  scattering in the state  $L = 0, S = 0$ , and  $J^\pi = 0^+$ . Calculations are performed with the three-cluster configuration  ${}^4\text{He}+d+d$ .

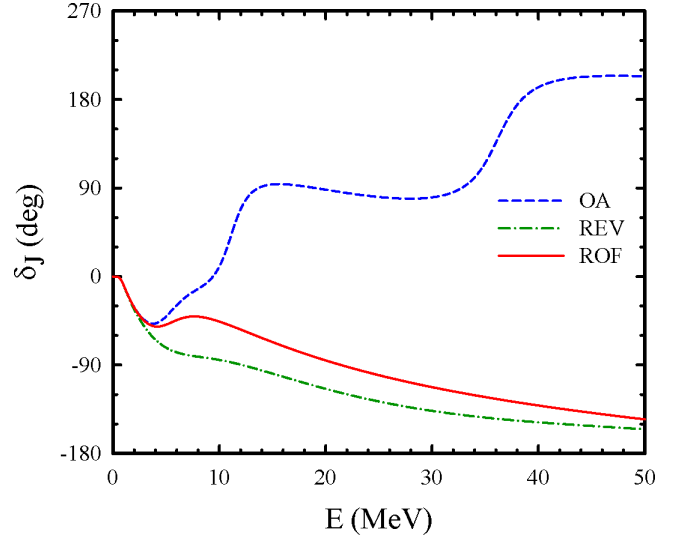


FIG. 19. Phase shifts of the  ${}^6\text{Li}+{}^4\text{He}$  scattering in the state  $L = 1, S = 1, J^\pi = 1^-$  obtained with three different approaches. The three-cluster configuration  ${}^4\text{He}+{}^4\text{He}+d$  is used in calculations.

$J^\pi = 0^-$  and  $J^\pi = 2^-$  generated by the coupling of the total orbital momentum  $L = 1$  with the total spin  $S = 1$ . Two Pauli resonance states were removed by eliminating two eigenfunctions of the norm kernel obeying the restriction  $\Lambda_\alpha \leq 0.2$ , and two oscillator functions with the restriction  $\langle n|n \rangle \leq 0.3$ . Noticeable deviation of the phase shifts obtained in the REV and ROF methods is seen at the energy region  $E > 3$  MeV. Such deviation can be explained by structure of the eigenfunctions and their relation to oscillator functions. If an eigenfunction is mainly represented by one oscillator function, then one may expect close results of both methods. If eigenfunction is spread over large number of oscillator functions, then results obtained with these two methods would be different. To prove this statement, we show in Fig. 21 eigenfunctions  $\|U_n^\alpha\|$  of the norm kernel as a function of  $n$  for two different cases with two Pauli resonance states. We selected cases for elastic  ${}^6\text{Li}+{}^4\text{He}$  scattering with quantum numbers  $L = S = 1, J^\pi = 1^-$  and  $L = 0, S = 1, J^\pi = 1^+$ . The phase shifts for them are shown in Figs. 19 and 20. Figure 21 demonstrates that, for the  $J^\pi = 1^-$  state, a large number of oscillator functions participate in the formation of eigenfunctions  $U_n^1$  and  $U_n^2$ , while, for the  $J^\pi = 1^+$  state, the lowest oscillator functions with  $n = 0$  and  $n = 1$  totally dominate in the corresponding eigenfunctions  $U_n^1$  and  $U_n^2$ . Similar dominance of oscillator function with the quantum number  $n = 0$  in the eigenfunction  $U_n^1$  are observed in all cases, when phase shifts obtained with the REV and ROF are coincide.

In Table V we show effects of eliminated eigenfunctions and oscillator functions on parameters of bound and resonance states. These results are obtained for the  $1^+$  states in  ${}^{10}\text{B}$ . By increasing  $\Lambda_{\min}$  ( $O_{\min}$ ) from zero to a certain value, indicated in the second column of Table V, we manage to eliminate one, two, and three eigenfunctions (oscillator functions). In the fourth column of Table V, we demonstrate how eliminated eigenfunctions and oscillator functions affect the energy of the

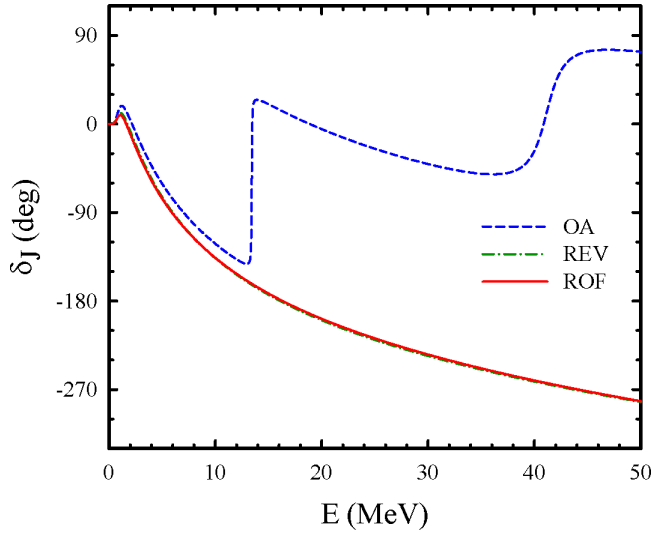


FIG. 20. Phase shifts of the elastic  ${}^6\text{Li} + {}^4\text{He}$  scattering with  $J^\pi = 1^+$  calculated within three approximations. Calculations are performed with the three-cluster configuration  ${}^4\text{He} + {}^4\text{He} + d$ .

$1^+$  bound state of  ${}^{10}\text{B}$ . In Fig. 22 we show effects of eliminated functions on the  ${}^6\text{Li} + {}^4\text{He}$  phase shift. By eliminating one eigenfunction or one oscillator function, we remove the lowest Pauli resonance state and change position (lower down) of the second resonance on approximately 6.5 MeV. However, the energy of the ground state is slightly changed after

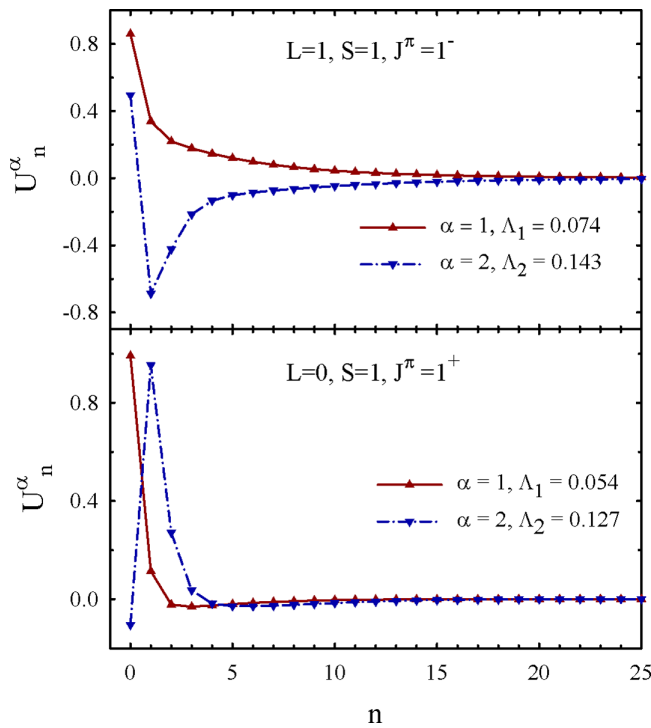


FIG. 21. Eigenfunctions  $U_n^\alpha$  of the norm kernel as a function of  $n$  for  $J^\pi = 1^-$  and  $J^\pi = 1^+$  states in  ${}^{10}\text{B}$ , considered as a two-cluster system  ${}^6\text{Li} + {}^4\text{He}$ . The three-cluster configuration  ${}^4\text{He} + {}^4\text{He} + d$  is involved in calculations.

TABLE V. Evolution of the  $1^+$  bound and resonance states in  ${}^{10}\text{B}$ . The energies and widths are in MeV.

Method	$\Lambda_{\min}/O_{\min}$	$N_f$	$E_{\text{GS}}$	$E$	$\Gamma$	$E$	$\Gamma$
OA	0.0	100	-2.477	13.427	0.056	41.144	2.751
REV	0.1	99	-2.280	—	—	34.539	3.503
ROF	0.1	99	-2.264	—	—	34.826	3.684
REV	0.2	98	-1.527	—	—	—	—
ROF	0.2	98	-1.183	—	—	—	—
REV	0.7	97	-0.132	—	—	—	—
ROF	0.7	97	0.526	—	—	—	—

removing one function. When we remove two eigenfunctions or two oscillator functions, both Pauli resonance states are disappeared. Two removed eigenfunctions increase the energy of the bound state by 0.9 MeV, while two removed oscillator functions increase the energy by  $\approx 1.3$  MeV.

As we indicated above, the oscillator functions with small values of the quantum number  $n$  and eigenfunctions with small values of index  $\alpha$  describe the most compact two-cluster configurations. It is interesting to analyze effects of their deletion on the energies of bound states and a shape resonances, if they appear. For this aim, we collected in Table VI the energies of bound and resonance states. In many cases, the elimination of the oscillator functions leads approximately to the same results as with the elimination of the eigenfunctions.

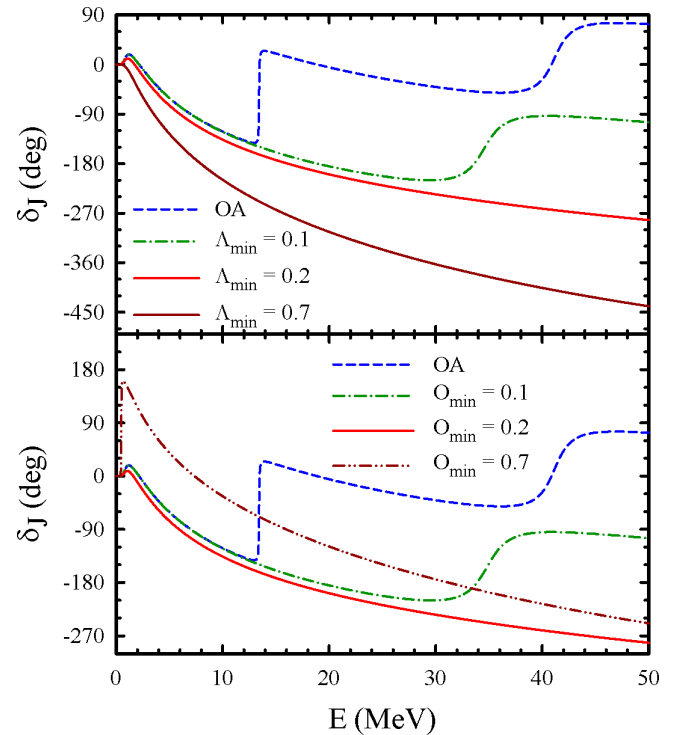


FIG. 22. Phase shifts of the elastic  ${}^6\text{Li} + {}^4\text{He}$  scattering obtained with different values of  $\Lambda_{\min}$  (the upper part) and  $O_{\min}$  (the lower part). Calculations are performed with the three-cluster configuration  ${}^4\text{He} + {}^4\text{He} + d$ .

TABLE VI. Effects of removed eigenfunctions and oscillator functions on the energies of bound and shape resonance states.

Nucleus	Channel	$J^\pi$	Parameter	OA	REV	ROF
${}^7\text{Li}$	${}^4\text{He} + {}^3\text{H}$	$3/2^-$	$N_f$	100	99	99
			$E_{\text{GS}}, \text{MeV}$	-1.127	-1.105	-1.064
${}^8\text{Be}$	${}^6\text{Li} + d$	$0^+$	$N_f$	100	99	99
			$E_{\text{GS}}, \text{MeV}$	-18.971	-15.281	-14.426
			$E, \text{MeV}$	0.153	0.374	0.352
	$2^-$	$\Gamma, \text{MeV}$	0.013	0.485	0.371	
		$N_f$	100	99	99	
		$E, \text{MeV}$	0.800	0.825	0.805	
${}^{10}\text{B}$	${}^6\text{Li} + {}^4\text{He}$	$1^+$	$\Gamma, \text{MeV}$	0.738	0.957	0.762
			$N_f$	100	98	98
			$E_{\text{GS}}, \text{MeV}$	-2.477	-1.527	-1.183

At the end of this section we made preliminary conclusions concerning the REV and ROF methods. In all cases, presented above, both methods completely remove all detected Pauli resonance states. In many cases, both methods give close results for phase shifts. In some cases, phase shifts are somewhat different. Such a difference, as we demonstrated, appear, when eigenfunctions of the norm kernel are spread over a large number of oscillator functions. In other words, removed eigenfunctions and removed oscillator functions are quite different. When results of both methods coincide, the removed eigenfunctions are presented mainly by removed oscillator functions.

We demonstrated that, the ROF method formulated in this paper, is an alternative method to the one suggested by Kruglanski and Baye. Advantage of the ROF is that it does not require a diagonalization procedure of the norm kernel matrix and then a transformation of matrix of the Hamiltonian to a new representation. This procedure is time-consuming when a large number of basis functions are involved. We also demonstrated that oscillator representation is appropriate tool for studying effects of the Pauli principle on kinematic (matrix of the norm kernel) and the dynamics (matrix of the Hamiltonian) of two- and many-cluster systems.

## VI. CONCLUSIONS

Properties of Pauli resonance states in the two-body continuum of the light nuclei  ${}^6\text{Li}$ ,  ${}^7\text{Li}$ ,  ${}^7\text{Be}$ ,  ${}^9\text{Be}$ , and  ${}^{10}\text{B}$  have investigated within the advanced version of the resonating group method. The advanced version employs a three-cluster configuration which allows one to consider in general case three two-body (binary) channels. One of constituents of a binary channel is considered as a two-cluster subsystem which provides us with a more correct description of the nuclei having distinct two-cluster structures and a small separation energy. The wave functions of two-cluster subsystem are obtained by solving the appropriate Schrödinger equation. In the advanced version, we employed the square-integrable bases—Gaussian and oscillator bases. Gaussian

basis is used to describe relative motion of two clusters in two-cluster subsystem and is very efficient in obtaining wave functions of bound states with a minimal number of basis functions. The oscillator basis is used to study interaction of the third cluster with two-cluster subsystem. It allows us to implement proper boundary condition for discrete and continuous spectrum states. It was demonstrated that oscillator basis is suitable tool to study effects of the Pauli principle and to reveal nature of the Pauli resonance states.

It was demonstrated that the advanced form of a two-cluster subsystem is the origin of the Pauli resonance states. More precisely, an advanced form of wave function of two-cluster subsystem is responsible for appearance of the Pauli resonance states.

It has been shown that the Pauli resonance states appear at the relatively high energy  $E > 11$  MeV. Some of these resonance states are very narrow resonance states; however, major part of them are broad resonance states. The most populated area of resonance states lies in the interval  $16 < E < 21$  MeV. Two dense area of widths of resonance states are located in intervals  $0.008 < \Gamma < 0.22$  MeV and  $0.9 < \Gamma < 1.2$  MeV.

It was found that the oscillator functions with minimal value of the quantum number  $n$  (the number of radial oscillator quanta) dominates in resonance wave functions. These basis functions yield very small values of the diagonal matrix elements  $\langle n|n \rangle$  of the norm kernel. It was also demonstrated that the very narrow Pauli resonance states can be detected by using a very small number of oscillator functions: from three to five functions.

We have established that the Pauli principle predetermine appearance of the Pauli resonance states by creating almost forbidden states; however, energies and widths of the Pauli resonance states are mainly formed by nucleon-nucleon forces.

We found that the number of Pauli resonance states for the given  $J^\pi$  state, discovered within the advanced version of the RGM, coincides with the number of the Pauli forbidden states determined in the standard version of the RGM.

One of the main conclusions of the present paper is that one needs to find the proper definition of the Pauli forbidden and Pauli allowed (fully or partially) states. Standard or a formal definition for Pauli forbidden states is that the eigenvalues for them should be equal zero  $\Lambda_\alpha = 0$ . Then the Pauli allowed states should have  $\Lambda_\alpha > 0$ . However, the carried out analysis leads us to the conclusion that, for light nuclei with the two-body clusterization, the border between forbidden and allowed states is  $\Lambda_{\min} = 0.2$ . It was also shown that oscillator functions  $|n\rangle$  which generate the diagonal matrix elements of the norm kernel  $\langle n|n \rangle \leq O_{\min} = 0.2$ , can be considered as the Pauli forbidden states. By removing of the Pauli forbidden states, one eliminates the Pauli resonance states and causes minor effects on the energy of bound states and the energy and width of the shape resonance states if they exist. We have not found universal values of  $\Lambda_{\min}$  and  $O_{\min}$  for all light nuclei, which have been considered.

As for perspective of this work. In the present paper, we have restricted ourselves to the single-channel approximation



to reveal the Pauli resonance states and find main factors responsible for the formation of such states. In the future, we are planning to consider the appearance of the Pauli resonance states in many-channel systems and how the REF and ROF can help to eliminate them. Many-channel cases are specially interesting since small eigenvalues of the norm kernel can appear due to a strong overlap of basis functions belonging to different channels. This strong coupling is not directly related to the Pauli principle. This makes the problem more attractive and challenging.

## ACKNOWLEDGMENTS

We thank K. Katō for stimulating discussions and encouraging support. This work was supported in part by the Program of Fundamental Research of the Physics and Astronomy Department of the National Academy of Sciences of Ukraine (Project No. 0122U000889) and by the Ministry of Education and Science of the Republic of Kazakhstan, Research Grant IRN: AP 09259876. V.S.V. is grateful to the Simons foundation for financial support (Award No. 1030284).

- 
- [1] D. Clement, E. W. Schmid, and A. G. Teufel, *Phys. Lett. B* **49**, 308 (1974).  
 [2] G. Spitz, K. Hahn, and E. W. Schmid, *Z. Phys. A* **303**, 209 (1981).  
 [3] H. Kanada, T. Kaneko, and M. Nomoto, *Prog. Theor. Phys.* **54**, 1707 (1975).  
 [4] H. Kanada, T. Kaneko, and S. Saito, *Prog. Theor. Phys.* **54**, 747 (1975).  
 [5] T. Fliessbach and H. Walliser, *Nucl. Phys. A* **377**, 84 (1982).  
 [6] H. Kanada, T. Kaneko, and Y. C. Tang, *Nucl. Phys. A* **380**, 87 (1982).  
 [7] D. J. Stubeda, Y. Fujiwara, and Y. C. Tang, *Phys. Rev. C* **26**, 2410 (1982).  
 [8] Y. Fujiwara and Y. C. Tang, *Phys. Rev. C* **27**, 2457 (1983).  
 [9] H. Walliser and T. Fliessbach, *Nucl. Phys. A* **394**, 387 (1983).  
 [10] H. Walliser, T. Fliessbach, and Y. C. Tang, *Nucl. Phys. A* **437**, 367 (1985).  
 [11] H. Kanada, T. Kaneko, and Y. C. Tang, *Phys. Rev. C* **38**, 2013 (1988).  
 [12] M. Kruglanski and D. Baye, *Nucl. Phys. A* **548**, 39 (1992).  
 [13] V. Kukulin, V. Krasnopol'sky, and J. Horáček, *Theory of Resonances. Principles and Applications* (Kluwer Academic, Dordrecht, 1989).  
 [14] H. Feshbach, *Ann. Phys.* **5**, 357 (1958).  
 [15] H. Feshbach, *Ann. Phys.* **19**, 287 (1962).  
 [16] V. S. Vasilevsky, F. Arickx, J. Broeckhove, and T. P. Kovalenko, *Nucl. Phys. A* **824**, 37 (2009).  
 [17] J. A. Wheeler, *Phys. Rev.* **52**, 1083 (1937).  
 [18] J. A. Wheeler, *Phys. Rev.* **52**, 1107 (1937).  
 [19] A. V. Nesterov, V. S. Vasilevsky, and T. P. Kovalenko, *Phys. Atom. Nucl.* **72**, 1450 (2009).  
 [20] A. V. Nesterov, V. S. Vasilevsky, and T. P. Kovalenko, *Ukr. J. Phys.* **59**, 1065 (2014).  
 [21] N. Kalzhigitov, V. S. Vasilevsky, N. Z. Takibayev, and V. O. Kurmangaliyeva, *Acta Phys. Pol. B* **14**, 711 (2021).  
 [22] H. Horiuchi, *Prog. Theor. Phys. Suppl.* **62**, 90 (1977).  
 [23] Y. Fujiwara and H. Horiuchi, *Prog. Theor. Phys.* **63**, 895 (1980).  
 [24] K. Kato, K. Fukatsu, and H. Tanaka, *Prog. Theor. Phys.* **80**, 663 (1988).  
 [25] K. Varga, Y. Suzuki, and R. G. Lovas, *Nucl. Phys. A* **571**, 447 (1994).  
 [26] K. Varga, Y. Suzuki, and Y. Ohbayasi, *Phys. Rev. C* **50**, 189 (1994).  
 [27] Y. A. Lashko, V. S. Vasilevsky, and V. I. Zhaba, *Phys. Rev. C* **109**, 045803 (2024).  
 [28] D. R. Thompson, M. LeMere, and Y. C. Tang, *Nucl. Phys. A* **286**, 53 (1977).  
 [29] A. U. Hazi and H. S. Taylor, *Phys. Rev. A* **1**, 1109 (1970).  
 [30] T. Myo, Y. Kikuchi, H. Masui, and K. Katō, *Prog. Part. Nucl. Phys.* **79**, 1 (2014).  
 [31] H. Horiuchi, K. Ikeda, and K. Katō, *Prog. Theor. Phys. Suppl.* **192**, 1 (2012).  
 [32] T. Myo and K. Katō, *Prog. Theor. Exp. Phys.* **2020**, 12A101 (2020).